

CELL BIOLOGY

Ketogenic diet induces p53-dependent cellular senescence in multiple organs

Sung-Jen Wei^{1,2}, Joseph R. Schell^{1,2}, E. Sandra Chocron^{1,2}, Mahboubeh Varmazyad^{1,2}, Guogang Xu^{1,2}, Wan Hsi Chen^{1,2}, Gloria M. Martinez^{1,2}, Felix F. Dong^{1,2}, Prethish Sreenivas^{1,2}, Rolando Trevino Jr.^{1,2}, Haiyan Jiang^{1,2}, Yan Du^{3,4}, Afaf Saliba³, Wei Qian^{5,6}, Brandon Lorenzana^{1,2}, Alia Nazarullah^{1,2}, Jenny Chang^{5,6}, Kumar Sharma^{3,7}, Erin Munkácsy^{1,2}, Nobuo Horikoshi^{1,2}, David Gius^{1,2*}

A ketogenic diet (KD) is a high-fat, low-carbohydrate diet that leads to the generation of ketones. While KDs improve certain health conditions and are popular for weight loss, detrimental effects have also been reported. Here, we show mice on two different KDs and, at different ages, induce cellular senescence in multiple organs, including the heart and kidney. This effect is mediated through adenosine monophosphate-activated protein kinase (AMPK) and inactivation of mouse double minute 2 (MDM2) by caspase-2, leading to p53 accumulation and p21 induction. This was established using p53 and caspase-2 knockout mice and inhibitors to AMPK, p21, and caspase-2. In addition, senescence-associated secretory phenotype biomarkers were elevated in serum from mice on a KD and in plasma samples from patients on a KD clinical trial. Cellular senescence was eliminated by a senolytic and prevented by an intermittent KD. These results have important clinical implications, suggesting that the effects of a KD are contextual and likely require individual optimization.

INTRODUCTION

High-fat, low-carbohydrate (ketogenic) diets have become increasingly popular over the past decades for both weight loss and other health conditions (1). The minimal consumption of carbohydrates during a ketogenic diet (KD) induces the liver to produce ketones (2, 3), which are subsequently used as an alternate energy source (1). KD has been shown to be effective in treating refractory epilepsy (4) and may also have beneficial effects against cancer (5) and neurodegenerative diseases (6, 7). In addition, multiple KD studies using murine models have shown anti-inflammatory effects (8, 9) and improvements in midlife longevity (10, 11) and neurological (12, 13), metabolic (14), and obesity (12) phenotypes. Conversely, there is also evidence that low-carbohydrate diets can be pro-inflammatory in mice (15, 16) and increase the risks of cardiac fibrosis (17, 18) and kidney damage (19). There is insufficient information regarding the mechanisms responsible for these divergent outcomes, which individuals may be at risk for adverse effects, or if any interventions could mitigate these risks.

It seems reasonable to suggest that the specific variables of the KD combined with those of the individual undergoing dietary intervention all contribute to determining the beneficial or detrimental effects. Important variables include the age of the individual and the duration and specific composition of the diet. Multiple studies suggest that the age at which dietary intervention is initiated may be important. For instance, 12-month-old mice put on a KD showed reduced midlife mortality and improved memory (10, 11) and skeletal muscle maintenance (20),

while, in contrast, mice starting a KD at 3 weeks of age showed impaired development (21). Potential side effects of long-term KD have also been reported (1, 17, 22, 23). In particular, children with intractable epilepsy, who clearly benefit from the use of a KD (4, 24, 25), were found to be at an increased risk for kidney stones, bone fractures, and growth disturbances when on a KD continuously for more than 6 years (24, 26).

Here, we show on two different KDs that mice accumulate senescent cells in the normal tissue of multiple organs. We chose these two different KDs, Crisco versus cocoa butter-based, because these two diets contain very different ratios of saturated versus unsaturated fatty acids. KD-induced cellular senescence was not age-dependent and was observed in mice put on a 21-day KD starting at 6, 16, 24, and 52 weeks of age. Mice on a KD showed elevated p53, mediated by phosphorylated adenosine monophosphate-activated protein kinase α (pAMPK α) and mouse double minute 2 (MDM2) inactivation through caspase-2 cleavage, leading to induction of p21 and cellular senescence. Markers of the senescence-associated secretory phenotype (SASP) were increased in mouse serum following a 21-day KD as well as in human plasma from individuals on a 6-month KD clinical trial at our institutions [University of Texas Health Science Center at San Antonio (UTHSCSA)]. Last, cellular senescence was prevented by administration of an intermittent KD (IKD) regimen. As cellular senescence has been implicated in the pathology of organ disease, our results have important clinical implications for understanding the use of a KD.

RESULTS

Two different KDs induce cellular senescence

C57BL/6 male mice at 35 to 42 days old (or roughly 6 weeks) and weighting at least 15 grams were randomly assigned to either a control diet (17% calories from fat, 25% from protein, and 58% from carbohydrate) or a KD (90.5% calories from fat, 9.2% from protein, and 0.3% from carbohydrate) (Table 1) fed ad libitum and then euthanized after

Copyright © 2024 The Authors, some rights reserved; exclusive licensee American Association for the Advancement of Science. No claim to original U.S. Government Works. Distributed under a Creative Commons Attribution NonCommercial License 4.0 (CC BY-NC).

¹Department of Radiation Oncology, Mays Cancer Center at UT Health San Antonio MD Anderson, Joe R. and Teresa Lozano Long School of Medicine, San Antonio, TX, USA. ²Barshop Institute for Longevity and Aging Studies at UT Health San Antonio, San Antonio, TX, USA. ³Center for Precision Medicine, UT Health San Antonio, San Antonio, TX, USA. ⁴School of Nursing, UT Health San Antonio, San Antonio, TX, USA. ⁵Houston Methodist Cancer Center, Houston, TX, USA. ⁶Houston Methodist Research Institute, Houston, TX, USA. ⁷Division of Nephrology, Department of Medicine, UT Health San Antonio, San Antonio, TX, USA.

*Corresponding author. Email: gius@uthscsa.edu

Table 1. Diet composition for the Teklad and Research Diets Inc. While the percentages of calories from fat were roughly the same in both KDs, the lipid compositions were quite different. The fatty acid composition of the Teklad Crisco-based KD was 14% saturated and 84% unsaturated, consisting of 10% palmitic (C16:0), 4% stearic (C18:0), 23% oleic (C18:1), 51% linoleic (C18:2), and 7 to 10% α -linoleic (C18:3). In contrast, the Research Diets Inc. cocoa butter-based KD was roughly 60% saturated and 40% unsaturated, made up of 0 to 4% myristic (C14:0), 25 to 34% palmitic (C16:0), 34 to 40% stearic (C18:0), 1% arachidic (C20:0), 0 to 4% palmitoleic (C16:1), 26 to 35% oleic (C18:1), and 2 to 3% linoleic (C18:2) fatty acids.

Diet	Inotiv Teklad	Research Diets Inc.		
% of calories	Control	Ketogenic	Control	Ketogenic
Carbohydrate	58%	0.3%	80%	0%
Protein	25%	9.2%	10%	10%
Fat	17%	90.5%	10%	90%
kcal/gram	3.1	6.7	3.8	6.7

7 or 21 days. The primary fat source in this KD was hydrogenated vegetable shortening (Crisco), with ~84% unsaturated fatty acids and 14% saturated. Both diets were manufactured by Teklad and were used for all the experiments in this study, except where otherwise specified. We verified that calorie consumption on both the control and KD was identical (Fig. 1A), although a slight increase in body weight was observed in mice on the KD after 21 days (fig. S1A). We also verified that mice on the KD were in ketosis (Fig. 1B).

Because cellular senescence has been implicated in organ disease, including in the heart and kidneys (27–29), we assayed for a widely used biomarker, senescence-associated β -galactosidase (SA- β -gal) and found a significant increase after both 7- and 21-day KD in the heart (Fig. 1C), kidney (Fig. 1D), liver (fig. S1B), and brain (fig. S1C), compared to control. To verify that the apparent increase in cellular senescence was caused by KD, and not by a specific diet composition, including the percentages of saturated versus unsaturated fatty acids, we put mice on a cocoa butter-based KD from Research Diets Inc. (90% calories from fat, 10% from protein, and 0% from carbohydrate), with roughly 40% unsaturated fatty acids and 60% saturated. For this experiment, control mice were put on a protein-matched diet also from Research Diets Inc. (10% calories from fat, 10% from protein, and 80% from carbohydrates) (Table 1). Both the control and KD were fed ad libitum, and no difference in body weight was observed between the two groups over 21 days (fig. S1D). Serum ketone levels were also significantly increased on this KD (fig. S1E), and we saw elevated SA- β -gal in the heart (Fig. 1E), kidney (Fig. 1F), liver (fig. S1F, left), and brain (fig. S1F, right).

The increase in SA- β -gal on a 21-day KD was confirmed in heart and kidney tissue by immunohistochemistry (IHC) staining with an anti-SA- β -gal antibody (Fig. 1, G and H). We also tested two additional biomarkers of cellular senescence (30, 31): histone protein macroH2A.1 (H2AY) and histone 3 lysine 9 trimethylation (H3K9me3). These experiments showed an increase in H2AY and H3K9me3 after a 21-day KD by IHC (Fig. 1, G and H, with higher magnification shown in fig. S1G), as well as by immunoblotting for H2AY (fig. S1, H and I), compared to controls. Pathology analysis showed that 15 to 20% of the cells in the heart and 10 to 15% of the cells in the kidney stained positive for SA- β -gal, similar to what has been reported in murine models of acute myocardial infarction (32), bleomycin-induced lung cell damage (33), and ionizing radiation (34).

Glucose and insulin tolerance tests (GTT and ITT, respectively) showed a deficit in glucose uptake following the 21-day KD compared to control (fig. S2A), with no significant change in insulin sensitivity

(fig. S2B), similar to what others have reported that KD can reduce glucose tolerance after several weeks, while insulin sensitivity is generally not affected until several months on a KD (35). Last, serum analysis by IDEXX BioAnalytics showed free fatty acids, triglycerides, low-density lipoproteins, and high-density lipoproteins were all elevated in mice on the 21-day KD (fig. S2C) compared to mice on the control diet, similar to what others have reported on a KD (36).

A KD activates p53 and induces p21

The p53 transcription factor plays a central role in multiple cellular stress responses, including growth arrest, DNA repair, apoptosis, and cellular senescence (37). To expand upon our initial findings, protein extracts from the heart (Fig. 2A), kidney (Fig. 2B), liver (fig. S2D), and brain (fig. S2E) were probed with an anti-p53 antibody. Compared to controls, all tissues showed a significant increase in p53 following both 7- and 21-day KD. We saw a similar increase in p53 phosphorylated at serine-18 (Fig. 2, A and B, and fig. S2, D and E), paralogous to phospho-p53^{Ser15} in humans, an established posttranslational modification that increases p53 transcriptional activity in response to cellular stress (38, 39), such as glucose deprivation (40). While it has been previously reported that a KD can increase p53 transcription (10) and acetylation (10, 11), these results extend those to also show increased p53 protein and phosphorylation levels.

We next examined p16 and p21, both of which have also been shown to be involved in cellular senescence. Significant up-regulation of p21, but not p16, was observed in the heart (Fig. 2A), kidney (Fig. 2B), liver (fig. S2D), and brain (fig. S2E) following a 21-day KD. We also confirmed increased protein levels of both p53 and p21 by IHC in the heart (Fig. 2C) and kidney (Fig. 2D). The number of cells with p21-positive nuclei, as measured from the IHC staining, was ~20% in the heart and 15 to 20% in the kidney, similar to SA- β -gal. Last, we used reverse transcription quantitative polymerase chain reaction (RT-qPCR) to measure changes in gene expression in kidney following 21-day KD and found that these approximated the observed changes in protein levels (Fig. 2E).

We also verified a physical interaction between p53 and a p53 DNA binding sequence by mixing tissue extracts with a biotin-labeled four-tandemly repeated p53 DNA binding sequence from the p21 promoter, followed by immunoblotting with anti-p53 antibody (Fig. 2F and fig. S2F). These results were further validated in vivo using a chromatin immunoprecipitation (ChIP) binding assay of p53 and phospho-p53 to two known binding sites in the p21 promoter in primary cells isolated from the heart (Fig. 2G) and kidney (Fig. 2H).

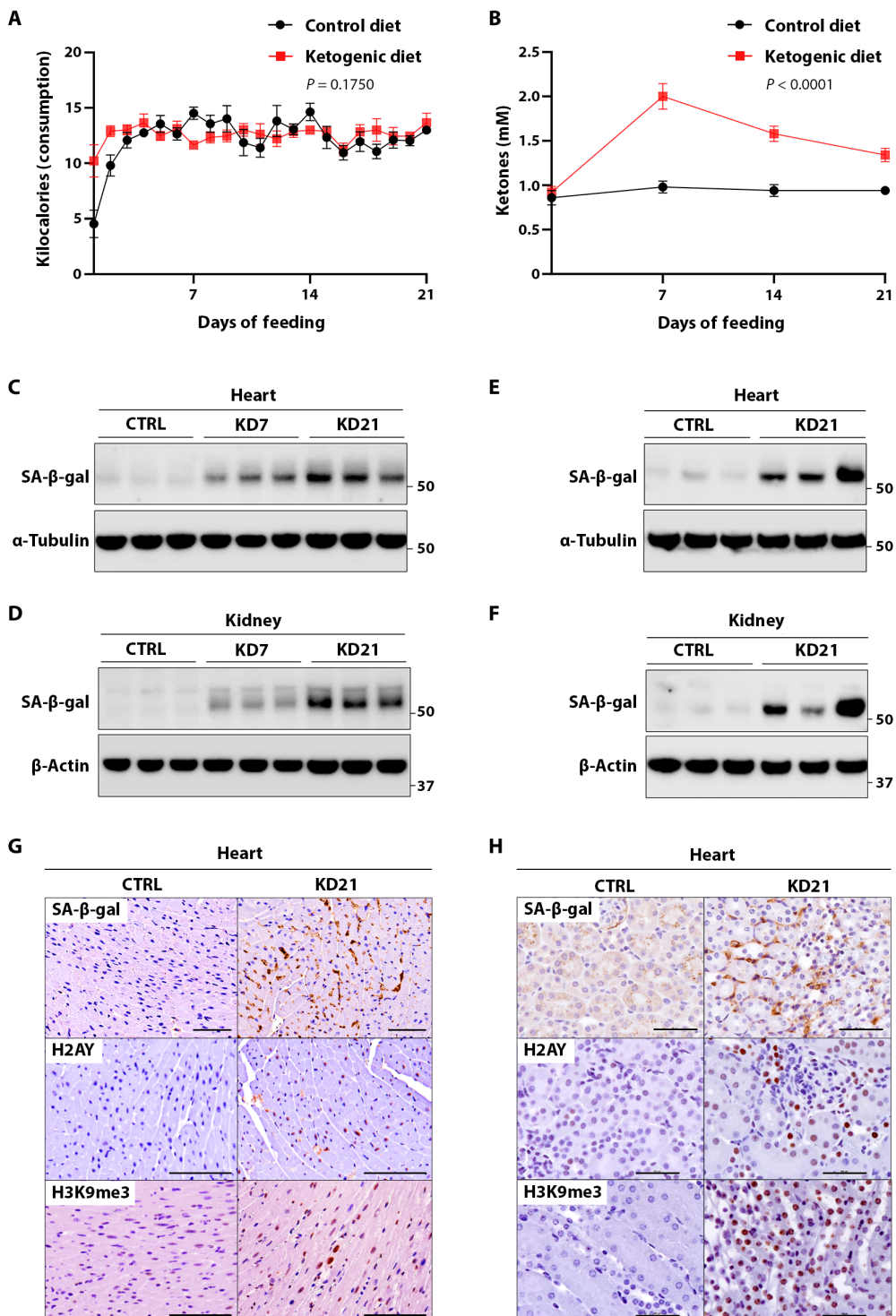


Fig. 1. Two different KDs induce cellular senescence. (A and B) Kilocalorie consumption (A) and serum ketone levels (B) in mice on control (CTRL) or Crisco-based KD ($n = 5$ mice per group). Data are represented as means \pm SEM. P values were calculated by two-way analysis of variance (ANOVA). (C and D) Immunoblots showing senescence-associated β -galactosidase (SA- β -gal) levels in heart (C) and kidney (D) tissue on control or 7- and 21-day Crisco-based KD ($n = 6$ mice per group). (E and F) Immunoblots show SA- β -gal in heart (E) and kidney (F) tissue on control diet versus 21-day cocoa butter-based KD ($n = 6$ mice per group). (G and H) Immunohistochemistry (IHC) staining for SA- β -gal, histone protein macroH2A.1 (H2AY), and histone 3 lysine 9 trimethylation (H3K9me3) in heart (G) and kidney (H) tissue on control versus 21-day Crisco-based KD ($n = 4$ mice per group). Scale bars, 100 μ m. All measurements are of distinct biological samples. Representative blots and images are shown.

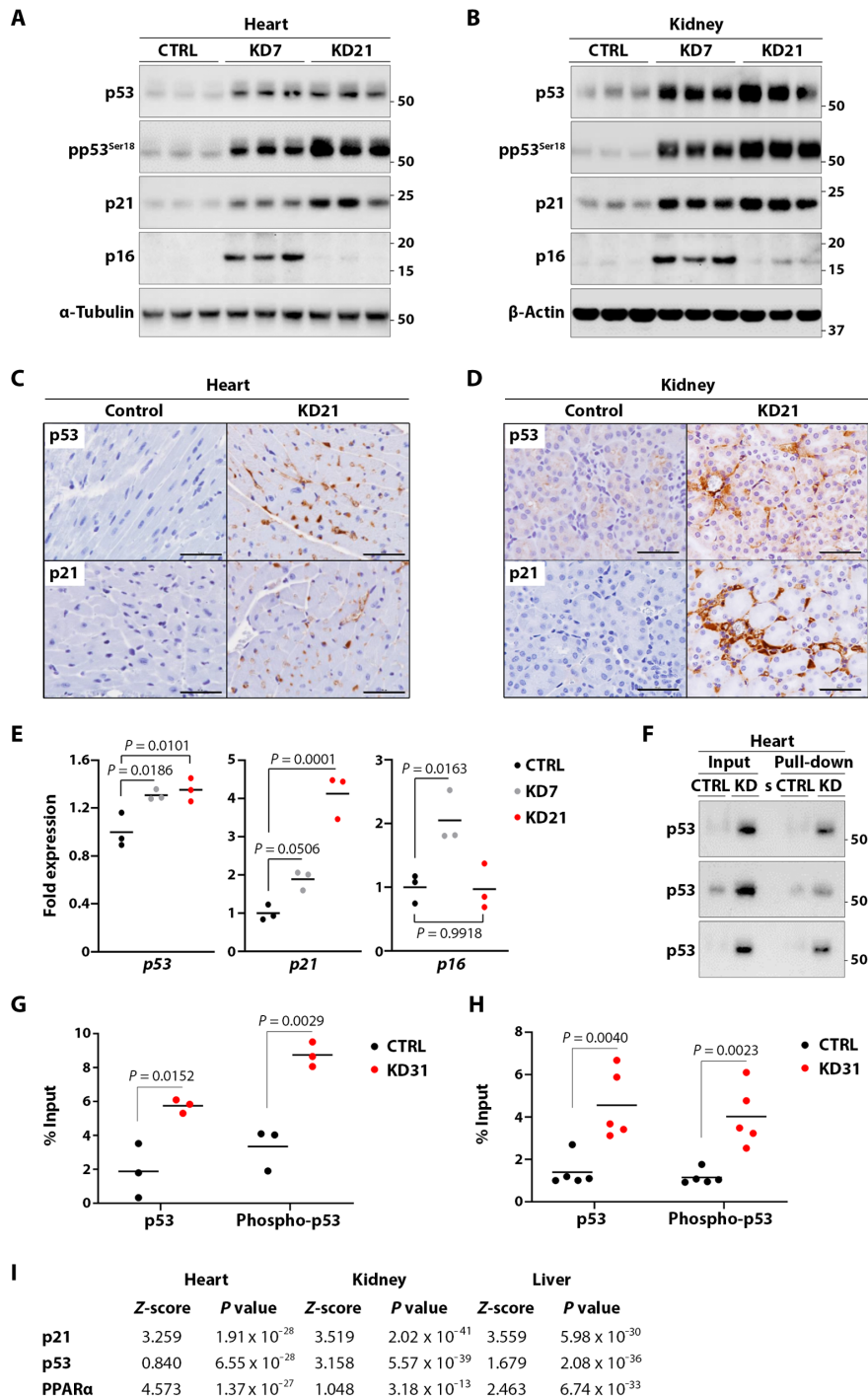


Fig. 2. A KD activates p53 and induces p21. (A and B) Immunoblots show p53, phospho-p53^{Ser18} (pp53^{Ser18}), p21, and p16 levels in heart (A) and kidney (B) tissue following control, 7-day KD, and 21-day KD ($n = 6$ mice per group). (C and D) IHC staining for p53 and p21 in heart (C) and kidney (D) tissue on control versus 21-day KD ($n = 4$ mice per group). Scale bars, 100 μ m. (E) Reverse transcription quantitative polymerase chain reaction (RT-qPCR) quantification of p53, p21, and p16 mRNA in kidney tissue from mice on the control diet, 7-day KD, and 21-day KD ($n = 3$ mice per group). P values were calculated by two-tailed Student's unpaired t test. (F) Kidney lysates were mixed with a biotin-labeled four-tandemly repeated p53 DNA binding sequence (from the p21 promoter), recovered using streptavidin agarose beads, and immunoblotted with p53 antibody ($n = 3$ mice per group). Lanes labeled "s" were left empty. (G and H) Chromatin immunoprecipitation (ChIP)-qPCR analysis shows binding of p53 and phospho-p53^{Ser18} at two known p53 binding sites within the p21 promoter region in heart (G) ($n = 3$ mice per group) and kidney (H) ($n = 5$ mice per group) cells isolated from mice on control and 31-day KD. P values were calculated by two-tailed Student's unpaired t test. (I) Total RNAs were isolated from heart, kidney, and liver tissues for RNA sequencing (RNA-seq) from mice on the control diet and on 21-day KD ($n = 3$ mice per group). Sequence reads were mapped with Hisat2 aligner and quantified by StringTie, and differential gene expression was identified by DESeq R. The resulting lists of hundreds of differentially expressed genes were processed by QIAGEN Ingenuity pathway analysis (IPA) software to identify activated upstream regulators. Representative blots and images are shown. PPAR α , peroxisome proliferator-activated receptor α .

In all of these experiments, we saw increased interaction of p53 following a KD, providing additional data suggesting that p53 acts via p21 to induce cellular senescence on KD.

To identify additional changes in signaling and transcription following a 21-day KD, RNA sequencing (RNA-seq) was done on heart, kidney, and liver tissue, and several hundred differentially expressed genes were identified. We used QIAGEN ingenuity pathway analysis (IPA) software to analyze these and identify enriched pathways and upstream regulators. This showed that p21, p53, and peroxisome proliferator-activated receptor α are activated upstream regulators on a KD (Fig. 2I) as shown by increased expression of their downstream targets compared to controls.

We also compared our RNA-seq data to an established list of 89 p53-regulated genes involved in cellular senescence (41) and found significant enrichment in all three tissues ($P < 0.0001$ by Fisher's exact test) (fig. S3, A to E). IPA analysis also showed an enrichment in genes, as shown by heatmaps, associated with cellular senescence (fig. S4, A to C). We confirmed the altered levels of several genes from both datasets by immunoblot analysis; specifically, cyclin A2, mitotic checkpoint serine/threonine-protein kinase, Forkhead box protein M1, and Lamin B1 were all decreased, while Serpine1 (PAI-1) was increased (fig. S4, D to F), as others have reported in senescent cells (42, 43). Last, IPA analysis identified multiple pathways that potentially contribute to the observed changes in metabolism and cellular senescence (fig. S4G).

KD-induced cellular senescence is dependent on p53 and p21

The above results delineate a pathway in which sustained KD activates p21 through p53, ultimately leading to cellular senescence in multiple organs. To determine the dependence of KD-induced cellular senescence on this pathway, we first tested p53 by measuring p21 and SA- β -gal in p53 knockout (KO) mice (*Trp53^{tm1Tgj}*) (44) following a 21-day KD. In contrast to control or wild-type (WT) mice, neither p21 nor SA- β -gal was up-regulated in p53 KO mice on KD (Fig. 3, A and B, and fig. S5, A and B). Likewise, while a 21-day KD induced p53, p21, and SA- β -gal in WT mice, as shown by IHC (Fig. 3C), we saw minimal to no elevation of these proteins in p53 KO mice (Fig. 3D). H2AY and H3K9me3 IHC staining was not observed in the p53 KO mice on a KD compared to p53 KO mice on control diet (fig. S5, C and D) or compared to WT mice on control diet or KD (Fig. 1, G and H). Last, we used RT-qPCR to further validate p21 and *glb1* (SA- β -gal) expression in heart (Fig. 3E) and kidney tissue (Fig. 3F) of p53 KO and WT mice following a 21-day KD.

Next, we tested the dependence of KD-induced cellular senescence on the increase in p21 by using a p21 inhibitor, UC2288, which decreases p21 mRNA independently of p53 (45). Starting on day 1 of a 21-day KD, UC2288 was administered every other day by oral gavage at a dose of 15 mg/kg. Compared to mice given vehicle only on a KD, mice given UC2288 exhibited significantly lower levels of p21 and SA- β -gal (Fig. 3, G and H, and fig. S5E), similar control diet mice. Together, these data indicate that KD-induced cellular senescence occurs through p53 up-regulation of p21.

A KD activates p53 through cleavage of MDM2

To further investigate the mechanisms underlying p53 activation on KD, we examined the nuclear-localized E3 ubiquitin ligase, MDM2, which promotes the nuclear export, cleavage, and degradation of p53 (46, 47). Mice on a KD exhibited significantly increased cleaved

MDM2 and reduced full-length compared to control mice (Fig. 4, A and B, and fig. S5, F to I). These data suggest that MDM2 inactivation may contribute to the stabilization and increase of p53 observed on KD. MDM2 is itself cleaved and inactivated by a complex known as the PIDDosome (48), which comprises p53-induced death domain protein 1 (PIDD1), receptor-interacting protein-associated interleukin-1 β converting enzyme homolog 1/C. elegans cell death protein 3 (ICH-1/CED-3) homologous protein with a death domain (RAIDD), and pro-caspase-2 (which is cleaved to active caspase-2) (49). Compared to controls, mice fed a 7- or 21-day KD showed elevated PIDD1, RAIDD, and cleaved (active) caspase-2 (Fig. 4, A and B, and fig. S5F).

We next tested whether KD-induced p53 signaling requires caspase-2 activity. benzyloxycarbonyl-Val-Asp(OMe)-Val-Ala-Asp(OMe)-fluoromethylketone (Z-VDVAD-FMK) is a selective caspase inhibitor, specifically targeting caspase-2, caspase-3, and caspase-7 (50–52). Mice were given Z-VDVAD-FMK (10 mg/kg) via intraperitoneal injection on day 1 of a 31-day KD and every second day thereafter. The mice receiving the caspase inhibitor showed greatly reduced levels of cleaved MDM2 and markers of p53-induced cellular senescence compared to those given vehicle only while on KD (Fig. 4, C and D). The expected decrease in caspase-2 activity was confirmed by an *in vitro* activity assay using heart (Fig. 4E) and kidney (Fig. 4F) tissue lysates. To rule out an undetected dependence on caspase-3 or caspase-7, we probed heart and kidney lysates with antibodies to cleaved caspase-3, caspase-7, and poly(adenosine 5'-diphosphate-ribose) polymerase, a downstream target (fig. S6, A and B). This confirmed that neither caspase-3 nor caspase-7 is activated by 7- or 21-day KD. Last, as further confirmation that caspase-2 is required for KD-induced cellular senescence, we put caspase-2 KO mice (53) on a 21-day KD and saw no increase in cleaved MDM2, p53, p21, or SA- β -gal compared to controls (Fig. 4, G and H, and fig. S6C). Together, our results provide evidence that a KD can inactivate MDM2 by caspase-2 cleavage and thereby induce cellular senescence via a p53 signaling axis.

A KD activates p53 through AMPK

Because AMPK is also an established activator of p53 (54–56), we examined total and pAMPK α levels following a 21-day KD. We found an increase in phosphorylation at AMPK α threonine-172 in both the heart (Fig. 5A) and the kidney (Fig. 5B) compared to control, with no difference in total AMPK α . Blocking AMPK activity throughout a 21-day KD with daily intraperitoneal injections of dorsomorphin (5 mg/kg), an established inhibitor of AMPK activity (57), prevented phosphorylation of p53^{Ser18} as well as induction of p21 and SA- β -gal (Fig. 5, C and D). These results suggest that AMPK activation is also required for KD-induced cellular senescence on a KD.

In addition to AMPK activity, we have shown that the PIDDosome, specifically caspase-2 activity, is required for the KD-induced increase in p53 and cellular senescence (Fig. 4). Because p53 has also been shown to regulate expression of Pidd1 (58), we next tested whether AMPK phosphorylation is required for up-regulation of the PIDDosome by blocking AMPK activity throughout a 21-day KD with daily intraperitoneal injections of dorsomorphin, an AMPK-specific chemical inhibitor. These mice did not show an increase in PIDD1, RAIDD, or cleaved MDM2 (Fig. 5, E and F) compared to untreated mice on the KD. These experiments indicate that AMPK activation is required for the increase in p53, as well as the PIDDosome, and imply a potential positive feedback loop fueled by an increase in Pidd1 expression, as previously reported (58).

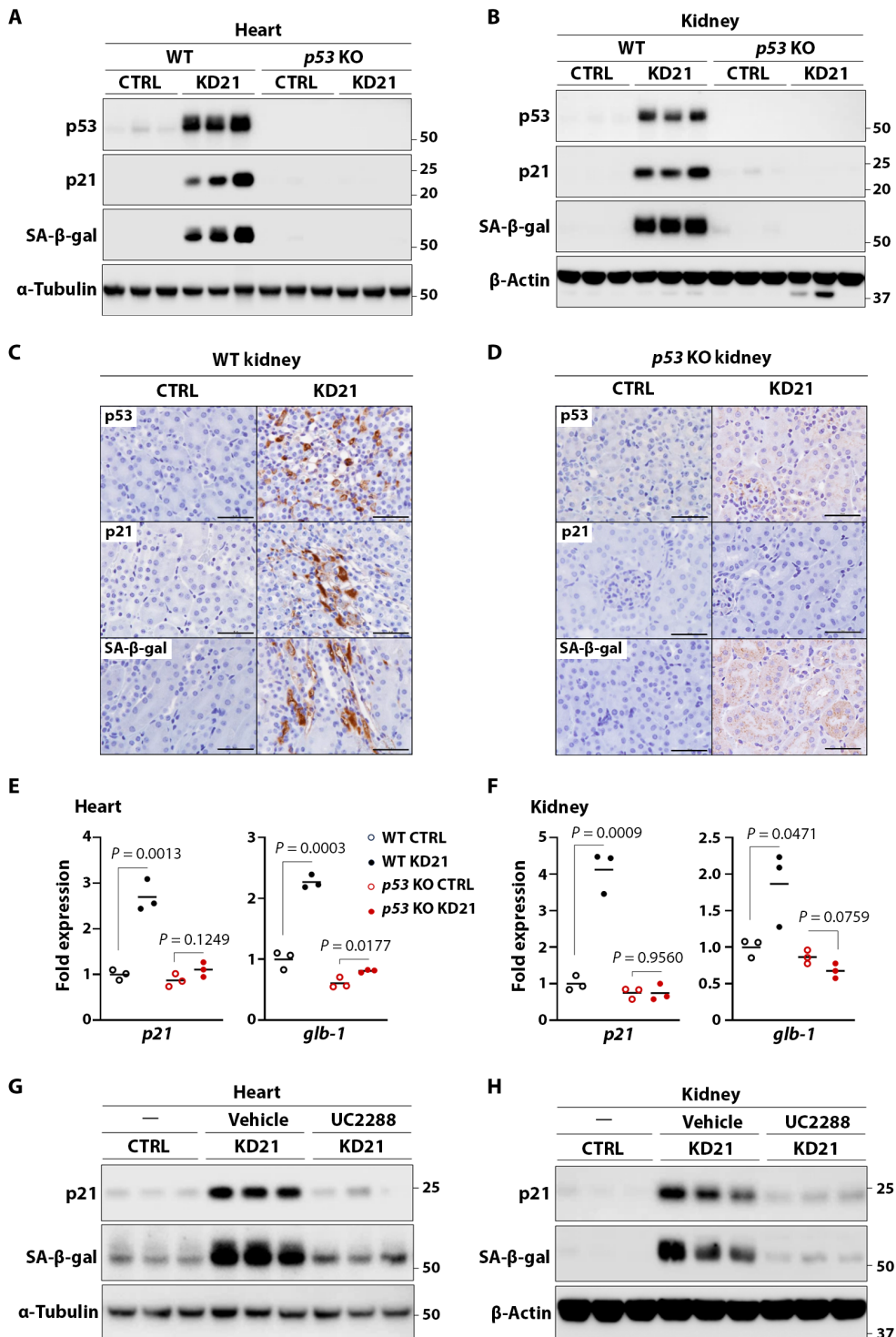


Fig. 3. KD-induced cellular senescence is dependent on p53 and p21. (A and B) Immunoblots from heart (A) and kidney (B) tissue of control [wild type (WT)] or homozygous *p53* knockout (*p53* KO) mice on control or 21-day KD ($n = 6$ mice per group). (C and D) IHC staining for p53, p21, and SA- β -gal levels in kidney tissue from WT (C) and *p53* KO (D) mice on control or 21-day KD ($n = 4$ mice per group). Scale bars, 100 μ m. (E and F) mRNA levels of *p21* and *g1b-1* in WT and *p53* KO mice on control versus 21-day KD in heart (E) and kidney (F) tissue ($n = 4$ mice per group). P values were calculated by two-sided Student's unpaired *t* test. (G and H) Immunoblots of heart (G) and kidney (H) tissue from mice on control or 21-day KD during which mice were given UC2288, which chemically inhibits p21, at 15 mg/kg or vehicle every other day by oral gavage ($n = 6$ mice per group). Representative blots and images are shown.

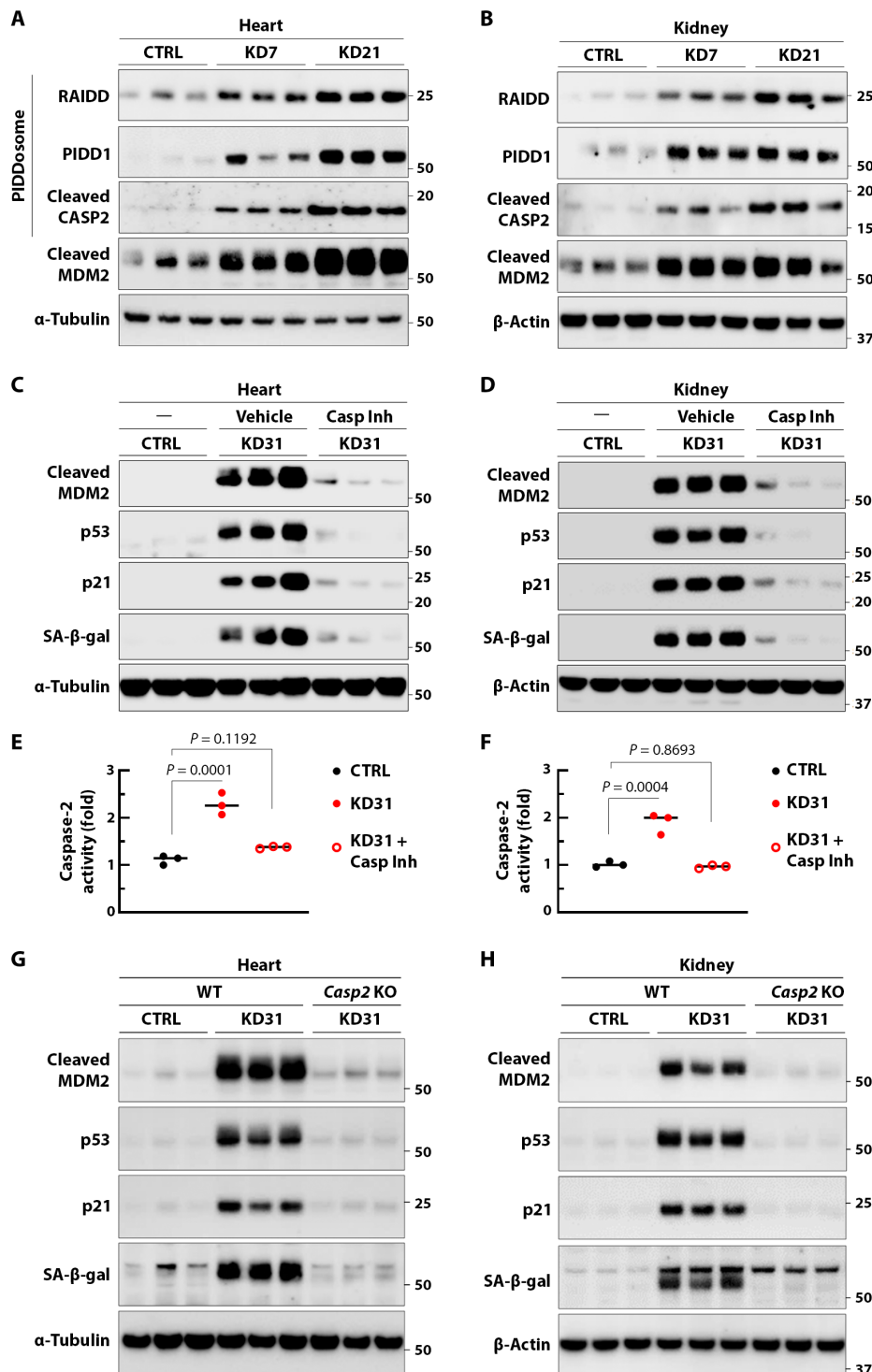


Fig. 4. A KD activates p53 through cleavage of MDM2. (A and B) Immunoblots show RAIDD, PIDD1, cleaved caspase-2, and cleaved MDM2 levels in heart (A) and kidney (B) from mice on control diet, 7-day KD, and 21-day KD ($n = 6$ mice per group). (C and D) Immunoblot analysis of heart (C) and kidney (D) tissue from mice on control or 31-day KD during which mice on a KD were also administered either a selective caspase inhibitor Z-VDVAD-FMK (Casp Inh) at 10 mg/kg or vehicle, every other day by intraperitoneal injection ($n = 6$ mice per group). (E and F) Caspase-2 activity in heart (E) and kidney (F) lysate on a 21-day KD. P values were calculated by one-way ANOVA followed by Dunnett's multiple comparisons test. (G and H) Immunoblots show cleaved MDM2, p53, p21, and SA- β -gal in heart (G) or kidney (H) from WT Casp2 and homozygous Casp2 KO mice on a control diet or 21-day KD ($n = 5$ mice per group). Representative blots are shown.

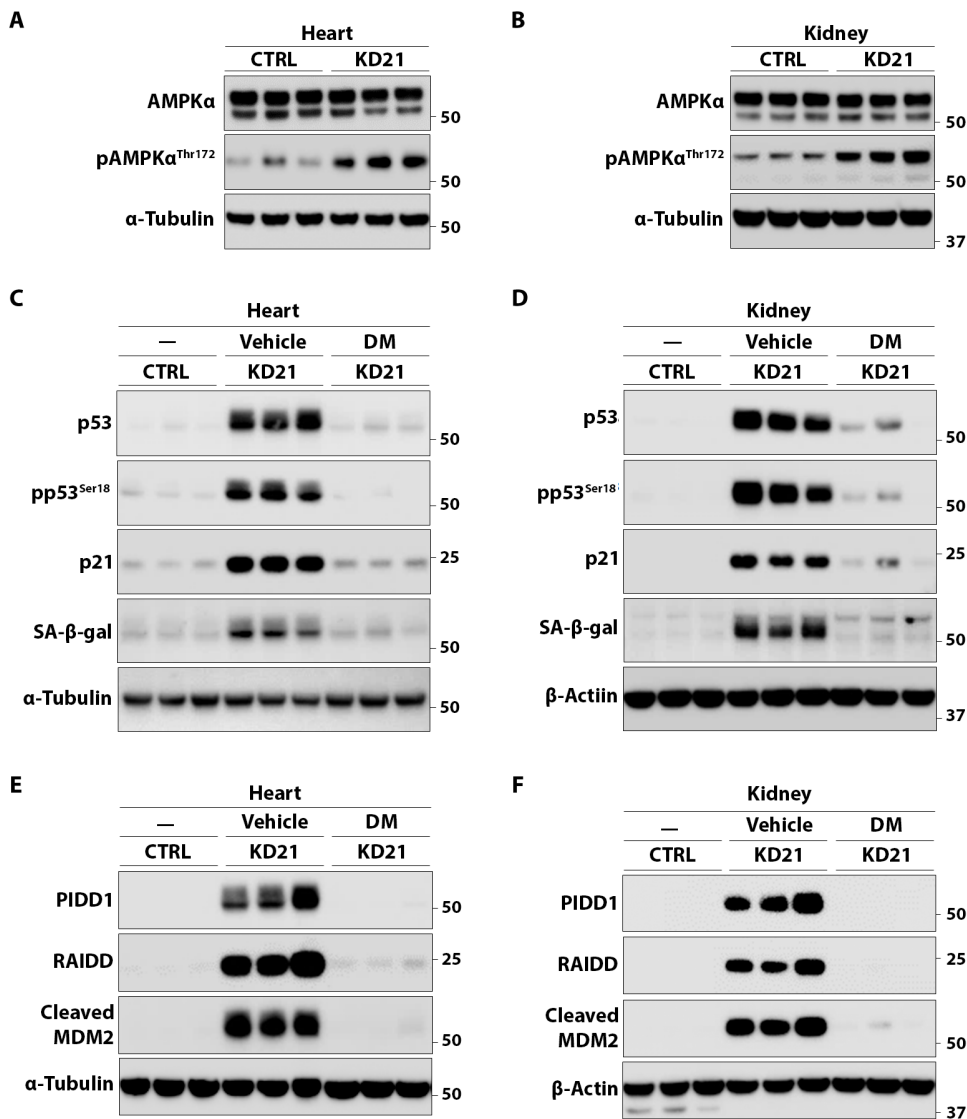


Fig. 5. A KD activates p53 through AMPK. (A and B) Immunoblots show total AMPK α and phospho-AMPK α -Thr¹⁷² (pAMPK α ^{Thr172}) levels in heart (A) and kidney (B) tissue in mice on the control diet or 21-day KD ($n = 6$ mice per group). (C and D) Mice on a 21-day KD were given dorsomorphin (DM), an inhibitor of AMPK activation, at 5 mg/kg or vehicle through daily intraperitoneal injection. Immunoblots show p53, pAMPK α ^{Thr172}, and SA- β -gal levels ($n = 6$ mice per group). (E and F) Mice on a 21-day KD were given DM, as above, and immunoblots show levels of PIDD1, RAIDD, and cleaved MDM2 ($n = 6$ mice per group). Representative blots are shown.

A KD induces markers of the SASP

Senescent cells can adversely affect adjacent cells and the tissue microenvironment by secreting pro-inflammatory cytokines (37). To address this in our KD model, we used enzyme-linked immunosorbent assay (ELISA) to measure biomarkers of the SASP (59, 60), specifically, tumor necrosis factor- α (TNF α), interleukin-1 β (IL-1 β), IL-6, and C-C motif chemokine ligand 5 (CCL5). While these cytokines are produced by various cells and have pleiotropic effects, they are frequently produced by senescent cells and have been shown to be pro-inflammatory (61). All were significantly increased in mouse sera following a 21-day KD (Fig. 6A). We also found similar up-regulation of SASP biomarkers in the heart, kidney, and liver tissue samples collected after 7- and 21-day KDs (fig. S6, D to F).

We next examined the relevance of these observations to humans by analyzing plasma samples from a published clinical trial by our

institution (62) in which patients of varying age, sex, and health condition were assigned to a KD, with fasting blood samples collected at the start of the trial (baseline) and after 3 and 6 months. Patients in this trial were monitored to confirm that they were in ketosis (62). In both male (Fig. 6B) and female patients (Fig. 6C), samples obtained after 6 months KD showed a significant increase in both TNF α and IL-1 β compared to baseline. We saw a similar trend in IL-6, with a significant increase in female patients after 6 months KD (Fig. 6C). In contrast, there was no change or only a modest increase in these pro-inflammatory biomarkers after 3 months on KD. These data support that a long-term KD can induce SASP in humans of varied age, sex, and health, similar to what we observed in mice on a 21-day KD. Last, we used a NIH 3T3 cell culture model that suggests it may be the increased lipids or lipoproteins, rather than the increase in ketone levels, that play a role in p53-induced cellular senescence on a KD (fig. S8A).

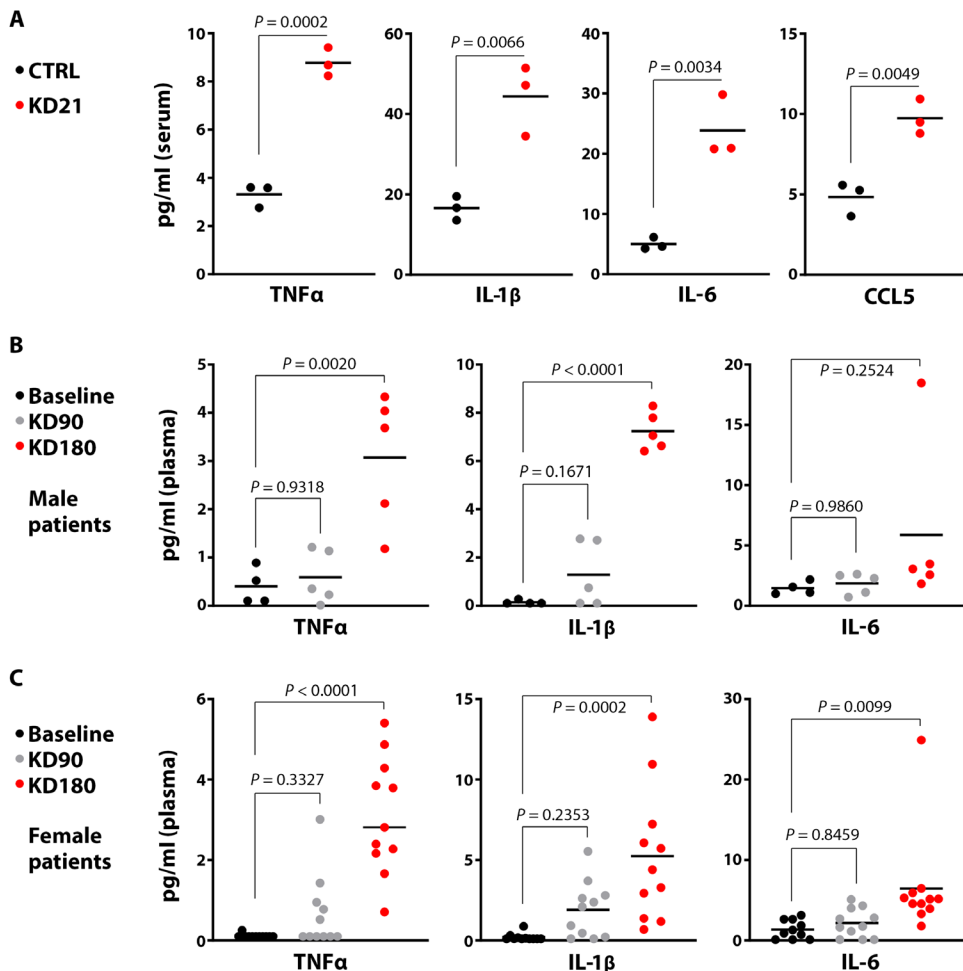


Fig. 6. A KD induces markers of the SASP. (A) Mouse serum TNF α , IL-1 β , IL-6, and CCL5, measured by ELISA in mice on a control or 21-day KD ($n = 3$ mice per group). P values were calculated by two-sided Student's unpaired t test. (B and C) TNF α , IL-1 β , and IL-6 measured by ELISA in plasma collected from male (B) ($n = 5$, except 4 at baseline) and female (C) ($n = 11$) patients at baseline and after 3 and 6 months on a clinical KD trial. P values were calculated by one-way ANOVA followed by Dunnett's multiple comparisons test.

A KD induces cellular senescence independent of age

Several studies suggest that the age at which one undergoes a KD plays a role in determining its effects, with several showing detrimental effects of KD during development (21, 24). Therefore, we sought to determine whether KD-induced cellular senescence is also observed in older mice. As such, we tested mice that were 16, 24, and 52 weeks of age when started on a 21-day KD. All mice, regardless of age, showed a significant increase in p53, p21, and SA- β -gal in both heart and kidney tissue on KD, compared to age-matched controls (Fig. 7, A to F), and comparable to mice starting the 21-day KD at 6 weeks of age.

Last, we have shown that two KDs with very different ratios of saturated versus unsaturated fatty acids both induce SA- β -gal (Fig. 1, C to F). The 21-day cocoa butter-based KD also increased p53, pp53 Ser18 , p21, cleaved MDM2, RAIDD, and PIDD1 in the heart, kidney, liver, and brain (fig. S7, A to D), as was also observed in mice on the Crisco-based KD. These data support that cellular senescence can be induced by sustained KD, independent of age or lipid composition, and is not an artifact of reduced dietary protein.

KD-induced cellular senescence is time-dependent and reversible

To further characterize cellular senescence on a KD, we euthanized mice after 4, 7, or 21 days on KD and assayed for p53, p21, and SA- β -gal. We found that all three proteins were minimally increased after 4 days on a KD, as compared to 7 and 21 days (Fig. 8, A and B). An important question is whether KD-induced senescent cells are cleared after the diet is stopped. Thus, to examine how long KD-induced cellular senescence persists, we put mice on a 7-day KD and euthanized them either immediately (as done in previous experiments) or after having returned to a normal control diet for 1, 2, or 3 weeks. We observed that upon return to normal control diet after a 7-day KD, p53, p21, and SA- β -gal levels are reduced after a week and continue to decrease toward control levels after 2 to 3 weeks on normal diet (Fig. 8, C and D).

An IKD does not induce cellular senescence

These data, showing that senescent cells can be cleared upon cessation of KD, led us to try interventions to either enhance clearance of senescent cells or prevent their accumulation while on KD. Navitoclax

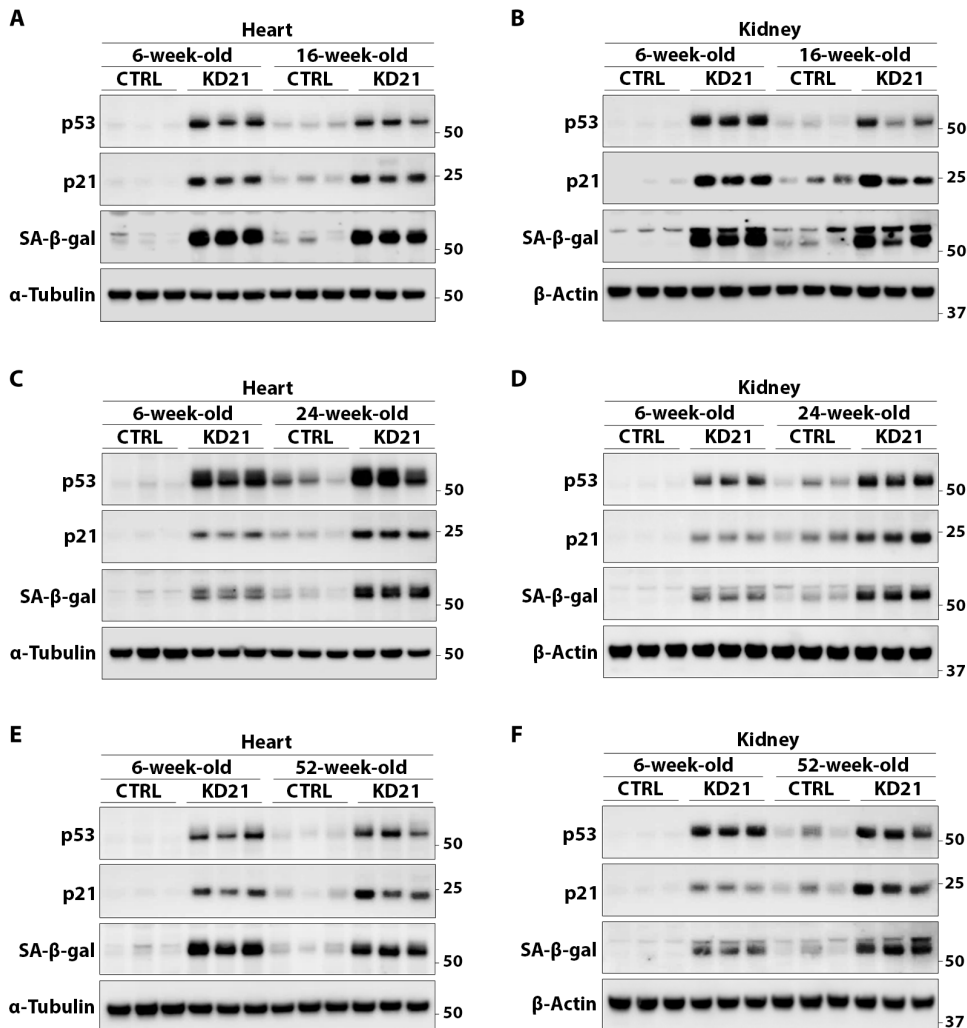


Fig. 7. KD induces cellular senescence in mice of different ages. (A to F) Immunoblot assays of p53, p21, and SA- β -gal levels in heart and kidney tissue from mice on control or KD for 21 days at the age of 6 weeks (controls), 16 weeks [(A) and (B)], 24 weeks [(C) and (D)], and 52 weeks [(E) and (F)] ($n = 5$ mice per group). Representative blots are shown.

(ABT-263) is a broad-spectrum senolytic that selectively removes senescent cells by binding to and inhibiting multiple antiapoptotic Bcl-2 family proteins, including BCL-2 and BCL-xL (63). To determine whether this senolytic would remove KD-induced senescent cells, mice were administered either ABT-263 at 50 mg/kg per day or vehicle by oral gavage for 7 days immediately following completion of a 21-day KD. Protein extracts from these mice suggest that ABT-263 treatment successfully cleared most of the senescent cells, while elevated p53, p21, and SA- β -gal were still observed in mice treated with vehicle only for 7 days after completing a 21-day KD and returning to normal control diet (Fig. 8, E and F, and fig. S8, B and C).

Several recent studies have reported benefits from various IKD protocols. An alternate-day KD improved cardiac function in a murine model of heart failure (64), while an alternate-week KD reduced midlife mortality, age-related memory loss, and other health issues in male mice (10). To evaluate whether an IKD would avoid p53 activation and cellular senescence, we placed mice on alternating 4-day KD and 7-day standard diet for three cycles (IKD), a 31-day KD (positive control), or a standard diet (negative control). In contrast to the sustained KD, the IKD did not increase p53 or cellular senescence (Fig. 8, G and H, and

fig. S8, D and E), nor did IKD increase SASP biomarkers in the tissues (fig. S8, F and G). These data potentially have important clinical application because they suggest that IKD may have fewer side effects than sustained KD while still potentially having a positive influence on health-related end points (10, 64).

DISCUSSION

It is increasingly evident that the effects of a KD are complex, and the health-related outcomes of its use likely depend on multiple factors (65). Some of the conflicting reports appear to revolve around whether a KD is pro- or anti-inflammatory. Multiple publications provide evidence that the primary ketone produced in ketogenesis, β -hydroxybutyrate (β -HB), may be anti-inflammatory (14, 66), suggesting that this could play a mechanistic role in the beneficial effects of KDs (8, 10). In contrast, others have shown KDs are pro-inflammatory and lead to organ disorders, including cardiac fibrosis and kidney damage (15–19, 67) perhaps due to the increase in lipids or lipoproteins, which have been shown previously to be detrimental (68). An important study suggests that diet duration may

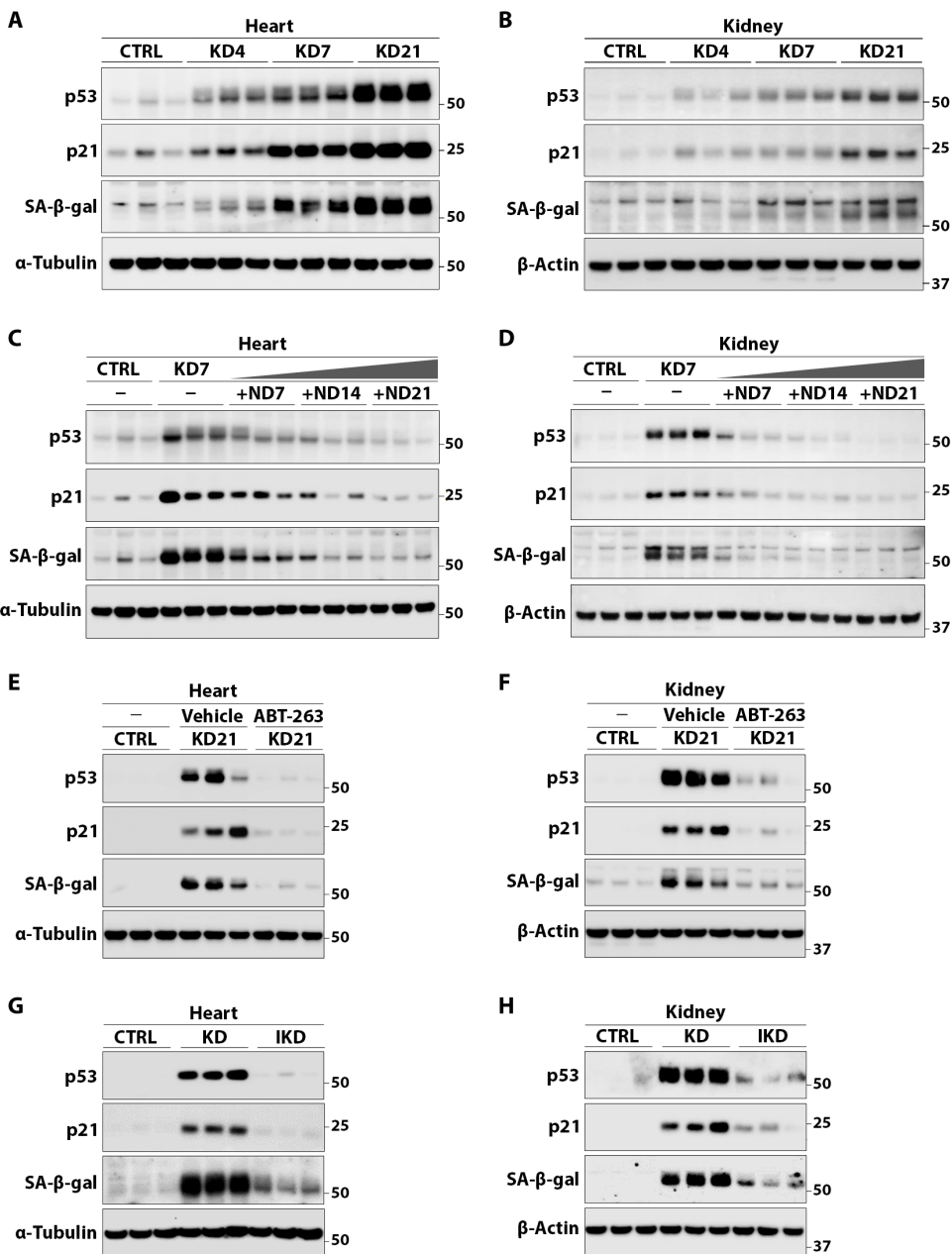


Fig. 8. Time course and interventions that prevent KD induced cellular senescence. (A and B) Immunoblots show p53, p21, and SA-β-gal immunoreactive protein levels in heart (A) and kidney (B) tissue from mice on control diet, 4-day KD, 7-day KD, and 21-day KD ($n = 5$ mice per group). (C and D) Immunoblot assays from mice placed on a 7-day KD and then switched to the normal control diet (ND) for 0, 7, 14, or 21 days ($n = 5$ mice per group). (E and F) Immunoblot analysis of heart (E) and kidney (F) proteins from mice on control or 21-day KD followed by administration of ABT-263 at 50 mg/kg or vehicle administered daily by oral gavage for 7 days ($n = 6$ mice per group). (G and H) Immunoblot analysis of heart (G) and kidney (H) tissue from mice on control diet, 31-day KD, or IKD consisting of three cycles of 4 days KD and 7 days control diet ($n = 6$ mice per group). Representative blots are shown.

be key in determining this outcome by showing a short-term KD improved murine metabolism through activation of tissue-specific resident immune cells, while a long-term continuous KD induced systemic inflammation, obesity, and glucose intolerance (9).

Our study builds on this idea and reveals a mechanism that may, at least in part, account for the detrimental effects of a long-term KD. Our experiments have shown that a KD can induce p53 signaling through AMPK activation combined with inactivation of MDM2 by

caspase-2 cleavage, ultimately leading to an increase in p21 and cellular senescence in multiple organs (fig. S9).

Because we observed that these changes in key organs such as the heart and kidneys, where the accumulation of senescent cells can contribute to systemic inflammation and toxicity (3, 18, 19), we believe that they have important clinical implications. In this regard, two publications showed a long-term KD promoted cardiac fibrosis and dysregulated mitochondrial function, due to chronic inflammation (18,

67), and while no mechanism involving cellular senescence was proposed, it remains an intriguing idea. Furthermore, it was recently published that KD-fed mice develop hepatic injury, steatosis, inflammation, glucose intolerance, and insulin resistance (22). In light of all these data and that our mice on a KD also showed reduced glucose tolerance, it could be hypothesized that metabolic dysfunction on a KD may lead to increased cellular senescence in specific conditions. There is an increasing consensus that the buildup of senescent cells, whether by increased induction or impaired clearance, contributes to age-related diseases and even aging itself (28, 29, 60, 69). Our analyses of SASP pro-inflammatory cytokines in patients suggest that cellular senescence may also be associated with sustained KD in humans.

IPA analysis of our RNA-seq data identified multiple pathways differentially regulated on KD that could potentially contribute to the observed alterations in metabolism and cellular senescence (fig. S4G). Several pathways involving DNA damage are up-regulated in multiple tissues while pathways involved in the cell cycle and replication are down-regulated. The down-regulation of these cell cycle and DNA replication pathways in particular suggests that there may be some difficulty for these cells to enter the synthesis phase (S phase). KD-induced disruptions to interphase have not been described yet in the literature but may hold some explanatory power for the success of the diet in other areas such as cancer therapy. Last, the differential regulation of genes involved in atherosclerosis is interesting because p53 is known to play a complex and tissue-dependent role in its progression (70).

Our study showed that an IKD can prevent the accumulation of senescent cells induced by sustained KD. This observation builds on that of others (10, 64), suggesting that an IKD may be more beneficial than a long-term continuous KD, perhaps by avoiding eventual pro-inflammatory activation (9). These data may be of clinical relevance because it could be surmised that the accumulation of senescent cells in children on a continuous KD, as used for refractory seizures, could play a role in the documented long-term side effects (71–73). We did test the reversibility of a 7-day KD because this has been reported to have beneficial effects in middle-aged mice when applied intermittently (10). Our results showed a significant reduction in p53, p21, and SA- β -gal after returning to a normal diet for 1-week, suggesting an IKD may be a potential alternative clinical intervention to a continuous KD.

An IKD could be especially relevant in the clinic, as this type of KD may be easier for patients to adhere to and could potentially offer many of the benefits of weight loss and improved health parameters without the risk of cellular senescence from sustained KD. In this regard, both an alternate-day and an alternate-week IKD have been reported to improve health parameters over a continuous KD in different murine models (10, 64), while a third study using a 3-day/week IKD reported attenuated improvements relative to continuous KD (74). Further research is clearly needed to determine whether and for what conditions an IKD could be beneficial in humans, as well as the optimum regimen.

The results of our *in vivo* murine experiments in this study, as well as those from other laboratories, reinforce that the effects of KD are complex, with both potential benefits and side effects likely due to multiple factors, including the timing, composition of the diet and the genetics, endocrine factors, and health conditions of the individual. As such, it is proposed that the use of a KD should be considered within the overall scope of personalized medicine, where the variables for each patient are taken into consideration to determine

who will, and who will not, benefit from this dietary intervention as well as the specific regimen to follow.

MATERIALS AND METHODS

Human participants

The clinical study was a single-center, 6-month, stratified, randomized controlled trial. A sample size of 60 adults with overweight/obesity aged 18+ years old were enrolled, including 20 who have overweight/obesity without type 2 diabetes or chronic kidney disease (protocol number HSC20190528H) and registered at <http://ClinicalTrials.gov> (ClinicalTrials.gov ID: NCT05071287). All of the patient samples were anonymized, and no patient information was provided for the data here. This clinical study has been previously published and contains all of the required information for the approval and presentation of clinical trials by the University of Texas Health Science Center at San Antonio (UTHSCSA) Institutional Review Board (62).

Mouse models

C57BL/6 (JAX strain no. 000664), B6.129S2-Trp53^{tm1Tyj}/J (JAX strain no. 002101), and B6.129S4-Casp2^{tm1Yuan}/J (JAX strain no. 007899) mice were obtained from the Jackson Laboratory and maintained in specific pathogen-free conditions at 21 ± 2°C with 12-hour:12-hour light:dark cycle in the Animal Facility at the Barshop Institute of UT Health San Antonio. The protocols for *Trp53* and *Casp2* genotyping were performed and optimized with reagents and conditions as recommended by the Jackson Laboratory. The sizes of PCR product for *Trp53* WT, heterozygote, and homozygote are 321, ~110 and 321, and ~110 base pairs (bp), respectively. The sizes of PCR product for *Casp2* WT, heterozygote, and homozygote are 304, 220 and 304, and 220 bp, respectively. To control for background effects in the experiments evaluating the dependency on *Trp53* and *Casp2*, homozygous KO and WT mice were derived from the heterozygous strains to be used as KO and control groups.

All mice had free access to a pelleted rodent diet and water. Mice were age-matched for all experiments. When all mice in a cohort weighed at least 15 g (35 to 42 days old), they were randomly divided into groups of four to six mice and fed either a KD or a control diet ad libitum for 7, 21, or 31 days or cycled (4-day KD alternating with 7-day control diet), as specified for each experiment. To assess the effects of a KD on mice of different ages, C57BL/6 male mice aged 16, 24, and 52 weeks were obtained from the Jackson Laboratory and assigned to either control or KD. Mice were euthanized, and tissues were harvested immediately upon the conclusion of the given diet, except in the experiments testing the persistence of KD-induced cellular senescence and the ABT-263 senolytic, where mice were put on control diet for a specified number of days after the KD.

The primary diet that we used to induce ketogenesis was a Crisco-based KD manufactured by Inotiv Teklad (TD.96355) and consisting of 90.5% calories from fat, 9.2% from protein, and 0.3% from carbohydrates (0% sucrose). For the control diet, we used the traditional formula LM-485 (no. 7012) from Teklad, which consists of 17% calories from fat, 25% from protein, and 58% from carbohydrates. For the alternate KD, we used a cocoa butter-based KD (D10070801) consisting of 90% calories from fat and 10% from protein, paired with a control diet (D19082304) consisting of 10% calories from fat, 10% from protein, and 80% from carbohydrates, both manufactured Research Diets Inc.

To measure food consumption, mice were singly housed and assigned to either control diet or KD for 21 days ($n = 5$ mice per group). Daily food consumption was measured daily at 10:30 a.m. by weighing food pellets. Mice were fed 14 kcal of the control diet and KD for the first 3 days. After 3 days, when the mice were growing and gaining weight, food quantity was then adjusted to 20 kcal so that the mice would have more available than they could eat in a 24-hour period.

The p21 attenuator, UC2288, was prepared in solution containing 5% dimethyl sulfoxide (DMSO), 40% polyethylene glycol 300 (PEG300), and 5% Tween 80 in H₂O. Male mice were put on a 21-day KD and administered either vehicle or UC2288 at 15 mg/kg via oral gavage starting on day 1 and continuing every second day thereafter (for a total of 11 administrations).

The selective caspase inhibitor, Z-VDVAD-FMK, was prepared in solution containing 5% DMSO, 40% PEG300, and 5% Tween 80 in H₂O. Male mice were put on a 31-day KD and administered either vehicle or Z-VDVAD-FMK at 10 mg/kg via intraperitoneal injection on day 1 and every second day thereafter (for a total of 16 administrations).

The selective AMPK inhibitor, dorsomorphin, was prepared in 1× phosphate-buffered saline (PBS). Male mice were put on a 21-day KD and administered dorsomorphin at 5 mg/kg via daily intraperitoneal injection starting on day 1 of the experiment (for a total of 21 administrations).

The senolytic ABT-263 was formulated in solution containing 5% DMSO, 40% PEG300, and 5% Tween 80 in H₂O. For the treatment of KD-induced senescence, male mice were fed with KD for 21 days, followed by the administration of vehicle or ABT-263 by oral gavage at 50 mg/kg per day for seven consecutive days (during which time they were fed control diet).

All animal experiments were carried out in compliance with National Institutes of Health (NIH) Guidelines for Humane Care and Use of Laboratory Animals and were approved by the UT Health San Antonio Institutional Animal Care and Use Committee.

Cell lines

Human embryonic kidney epithelial 293T cells were purchased from Life Technologies (Carlsbad, CA), and NIH 3T3 mouse fibroblasts were obtained from American Type Culture Collection (Manassas, VA). Cells were cultured in the respective recommended media at 37°C, 5% CO₂ (95% air), and 95% relative humidity. All cell lines used in this study were confirmed mycoplasma-free using the MycoAlert Mycoplasma Detection Kit (Lonza) and routinely checked for cell line identity using short tandem repeat genotyping as compared with the COGcell database (www.COGenCell.org).

Ketone body measurement

The level of ketone bodies in mice was quantitatively measured using the Keto-Mojo GK+ Bluetooth Glucose & Ketone Testing Kit (Keto-Mojo). The ketone body test strip was firmly inserted into the meter and then brought the tip of the strip to the droplet on the area of the saphenous vein of mice punctured by a 26-gauge needle. The strip draws the whole blood into the blood channel via capillary action. The meter starts to measure the amount of the β-ketone (β-HB) when the channel is completely full of blood. β-HB is converted by the enzyme β-HB dehydrogenase to acetooacetate. The magnitude of electrical current resulting from this enzymatic reaction is proportional to the amount of β-HB present in the sample.

Glucose and insulin tolerance tests

Mice were fasted for 6 hours before the GTT. They were not fasted before the ITTs. Both GTT and ITT were performed using a Contour Next EZ glucometer and glucose strips. A bolus of glucose (1.5 g/kg) or insulin (0.75 U/kg) was injected intraperitoneally into the mice. Glucose was then monitored over the following 2 hours.

Western blotting and imaging

Total protein lysate preparation from cells and organ tissues for pull-down or immunoblot are described (75, 76). Protein concentrations were determined by the bicinchoninic acid (BCA) Protein Assay Kit (Pierce), and 20 µg from each sample was separated by NuPAGE bis-tris 4 to 12% gradient SDS-polyacrylamide gel electrophoresis (PAGE) (Invitrogen) and transferred onto polyvinylidene difluoride membrane (Bio-Rad), probed with the primary antibodies, with horseradish peroxidase (HRP)-conjugated mouse or rabbit secondary antibodies (Cell Signaling Technology) and enhanced chemiluminescence (Thermo Fisher Scientific; SuperSignal West Femto Maximum Sensitivity Substrate).

Immunoblots were imaged by ProteinSimple FluorChem M using Auto Exposure feature that takes successively longer exposures of the membrane until an optimum exposure is achieved. Images are acquired in standard resolution, using 4 × 4 pixel binning (832 × 626-pixel images). Multichannel imaging captures fluorescent markers immediately adding chemiluminescent. The system includes three tools to enhance visibility of the results: brightness control (using non-linear gamma adjustment), exposures view, and color inversion. Densitometric analysis of protein quantitation was determined by ImageJ software v0.5.5 (NIH; <http://imagej.nih.gov/ij>, Java 1.8.0 - internal).

Immunohistochemistry

IHC staining for five mouse proteins (SA-β-gal, H2AY, H3K9me3, p53, and p21) was done at the Dr. Mary and Ron Neal Cancer Center, Houston Methodist. Tissue blocks of formalin-fixed, paraffin-embedded mouse tissues were processed by the Laboratory Medicine core, UT Health San Antonio using the standard methods. Tissue sections were fixed in 3% hydrogen peroxide followed by proteinaceous blocking solution (Avidin/Biotin Blocking Kit). Tissue sections were incubated with the indicated antibodies (see table S1), followed by addition of secondary antibody with EnVision+ System, HRP polymer (mouse or rabbit) and diaminobenzidine (DAB) substrate (Dako), and DAB sparkle (Biocare). When adequate color development was seen, slides were washed in water to stop the reaction, counterstained with Meyer's hematoxylin (Dako), and covered with a Permount mounting medium (Richard-Allan Scientific). The micrographs were taken under a light microscope (Leica). Representative images are shown.

Quantitative PCR analysis of mRNA expression

Total RNAs were extracted and purified from mouse organ tissues or cells using TRIzol reagent (Invitrogen) and the RNeasy Mini Plus Kit (QIAGEN), and cDNA was prepared with the High-Capacity cDNA Reverse Transcription Kit plus RNase inhibitor (Applied Biosystems) per instructions. qPCR primers used are listed in table S1. We used 2× PowerUp SYBR Green Master Mix (Applied Biosystems) and MicroAmp Optical 384-Well Reaction Plate with Barcode using ABI QuantStudio 5 RT-PCR system (Applied Biosystems). qPCR thermal cycling was 2 min at 50°C, 10 min at 95°C, 15 s at 95°C, and 1 min at 60°C for 40 cycles. The ΔΔCT data were analyzed by QuantStudio Design & Analysis Software v1.5.1 (Applied Biosystems).

Gene cloning and mutagenesis

The total RNAs (1 µg) isolated from NIH 3T3 mouse fibroblasts were reverse-transcribed into single-stranded cDNA by the High-Capacity cDNA Reverse Transcription Kit (Applied Biosystems). The cDNA fragments encoding Trp53 were PCR-amplified by the Expand High Fidelity PCR System (Sigma-Aldrich). The double-stranded DNA fragment was digested with Sgf1 and Mlu1-HF restriction enzymes and sequentially inserted in-frame into the Sgf1 and Mlu1 restriction sites of pCMV6-entry-mycDDK (OriGene) mammalian expression vector using LigaFast Rapid DNA Ligation System (Promega). The DNA sequence was verified by Psomagen using an automated ABI-3730xl DNA Analyzer and ABI PRISM BigDye Terminator v3.1 Cycle Sequencing Kit (Applied Biosystems). All plasmids were prepared using Hi-Speed Plasmid Midi Kits from QIAGEN (Valencia).

Cell transduction

Transfection of 293T cells with empty vector control (*pCMV6-entry-mycDDK*) or mouse *Trp53* (*pCMV6-Trp53-mycDDK*) was conducted as described in the Amaxa's nucleofector Cell and Transfection Database (Lonza) using the Nucleofector 2b System of Amaxa (Lonza). After nucleofection, the cells were plated and incubated at 37°C for 48 hours. Total protein lysates were then extracted and analyzed by SDS-PAGE and immunoblotted with specific antibodies to confirm the protein expression.

Pull-down

For pull-down studies, 3 mg of protein lysates were incubated at 4°C overnight with biotin labeled four-tandemly repeated p53 DNA binding sequence (Biotin-TP53 4BS) and pulled down using the EZ-view Red Streptavidin Affinity Gels. The protein complexes were washed four times with modified 1× radioimmunoprecipitation assay (RIPA), eluted by glycine-HCl (pH 3.5), neutralized with tris-HCl/NaCl (pH 8.0), and then concentrated using Amicon Ultra-0.5 Centrifugal Filter Units (10-kDa molecular weight cutoff). The samples were resolved by 4 to 12% SDS-PAGE and immunoblotted with the indicated antibodies.

Chromatin immunoprecipitation

ChIP analysis was performed as previously described (77). Briefly, primary heart and kidney cells were dissociated from fresh isolated mouse tissues using the Multi Tissue Dissociation Kit 2 (no. 130-110-203) and the gentleMACS dissociator (no. 130-093-235) per the manufacturer's instructions (Miltenyi Biotec). Six million cells were fixed in 1% formaldehyde at room temperature for 15 min and the protein/DNA cross-linking reaction was stopped by adding 125 mM glycine for 5 min. The fixed cells were collected by centrifugation at 1250g for 3 min at 4°C and rinsed with cold PBS twice. Cell pellets were resuspended in complete shearing buffer with 700 µl of tris(hydroxymethyl) aminomethane + ethylenediaminetetraacetic acid (TE) protease inhibitors and phosphatase inhibitors and sonicated for 10 cycles, 30-s on/30-s off, at low power to shear cross-linked protein/DNA to an average size of 200 to 1000 bp with Bioruptor Pico (Diagenode). Aliquots of the sheared chromatin DNA were used as input. The chromatin extracts (200 µl) with protein/DNA fragments were adjusted to RIPA buffer (200 mM NaCl) and ChIP-ed at 4°C overnight with rotation using 5 µg of mouse anti-p53 (Cell Signaling Technology) or anti-phospho-p53^{Ser15} (Cell Signaling Technology) antibody. The normal mouse immunoglobulin G antibody was used as negative control. Followed by incubation with protein A-coated magnetic

beads for 6 hours at 4°C, the beads were washed four times with wash buffer RIPA buffer, RIPA buffer (200 mM NaCl), LiCl buffer, and TE. The beads were resuspended in 100 µl of TE, 2.5 µl of 10% SDS, and 5 µl of proteinase K (10 mg/ml) and incubated overnight (65°C). Fragments of chromatin DNA were washed, decross-linked, eluted, and enriched using Mini elute columns in 50 µl of elution buffer. The real-time qPCR (at 1:5 dilution ratio) reactions were performed with two sets of *Cdkn1a* (p21) mouse promoter primers (site 1, 1.9 kb; and site 2, 2.8 kb) using ABI QuantStudioTM 5 Real-Time PCR system (Applied Biosystems). Relative occupancy values were calculated by determining the apparent ChIP efficiency (ratios of the amount of immunoprecipitated DNA to that of the input sample) and normalized to the level observed at a control region, which was defined as 1.0.

RNA-seq analysis

For RNA-seq, DNA-free total RNAs were isolated from heart, kidney, and liver tissues of mice on a 21 day of control or KD, using TRIzol reagent (Invitrogen) and the RNeasy Mini Plus Kit (QIAGEN) per manufacturer's instructions. The concentrations of total RNA samples were measured by NanoDrop. The quality of the total RNA samples was analyzed by Bioanalyzer. Samples (1 µg/10 µl) that pass quality control steps (RNA integrity number > 4) are then put through a series of steps to create a sequencing library by NovaSeq 6000 Illumina system using the appropriate sample preparation kit in the Genome Sequencing Facility, Greehey Children's Cancer Research Institute, UT Health San Antonio, San Antonio, Texas. Sequence reads were mapped to the UCSC/mm9 mouse genome using the HiSAT2 aligner, and quantification was carried out via StringTie. Differential expression analysis was done using the DESeq R package, and the following significance criteria were applied to the resulting gene list: FPKM > 1, adjusted *P* < 0.05, and fold change > 1.5. The differentially expressed genes were then processed using QIAGEN IPA software to determine pathway enrichment, upstream analysis, and significance scores.

Caspase-2 enzyme activity assays

The in vitro assay of caspase-2 enzyme activity was performed by Colorimetric Caspase-2 Assay Kit (Abcam) per the instructions. Total protein lysates were prepared from four organ tissues (heart, kidney, liver, and brain), isolated from the mice fed with a 31-day KD, and administered either vehicle or selective caspase inhibitor Z-VDVAD-FMK at 10 mg/kg via intraperitoneal injection on day 1 every second day thereafter. The tissue lysates (100 µg/50 µl each) were added to the 50 µl of 2× reaction buffer (containing 10 mM dithiothreitol) and incubated with 5 µl of the 4 mM acetyl-Val-Asp-Val-Ala-Asp-paranitroaniline (VDVAD-p-NA) substrate (200 µM final concentration) at 37°C for 1 hour. The samples were read at 405 nm in a 96-well plate reader (SpectraMax iD3, Molecular Devices). Fold increase in VDVAD-dependent caspase activity was determined by comparing the results of KD samples with the level of the control diet.

Enzyme-linked immunosorbent assays

ELISA immunoassays determined the concentrations of the SASP secretory proteins TNF α , IL-1 β , IL-6, and CCL5/RANTES in mouse serum and tissue lysates and human plasma using the appropriate the Cytokine/Chemokine ELISA Kit (see Table 2 for ELISA Kits and detection limits) in accordance with the manufacturer's instructions. Quantitative data were calculated and analyzed using linear dose-response standard curves obtained from purified recombinant proteins.

Table 2. Cytokine/Chemokine ELISA Kits and detection limits.

ELISA Kit	Detection limit
Human IL-1 β : BD OptEIA IL-1 β ELISA Set II (no. 557953)	0.3 pg/ml
Human IL-6: BD OptEIA IL-6 ELISA Set (no. 555220)	0.7 pg/ml
Human TNF α : BD OptEIA TNF ELISA Set (no. 555212)	0.3 pg/ml
Mouse CCL5: Sigma-Aldrich RANTES/CCL5 ELISA Kit (no. RAB007)	1 pg/ml
Mouse IL-1 β : R&D IL-1 beta/IL-1F2 Quantikine HS ELISA Kit (no. MHSLB00)	0.312 pg/ml
Mouse IL-6: R&D IL-6 Quantikine ELISA Kit (no. MHSTA50)	1.8 pg/ml
Mouse TNF α : R&D TNF-alpha Quantikine HS ELISA Kit (no. MHSTA50)	0.295 pg/ml

Statistical analysis

Except where otherwise noted, analyses were performed in Microsoft Excel v2308 or GraphPad Prism 10.1.0. Statistical differences were calculated as indicated by two-way analysis of variance (ANOVA), one-way ANOVA followed by Dunnett's multiple comparisons test, or unpaired Student's *t* test. *P* values were two-sided, and tests were considered significant at *P* < 0.05. All measurements were taken from distinct samples, and replicates are biological. All experiments were consistently repeatable. The number of replicates (mice) for each experimental group is given in the figure legends and the Supplementary Materials. In immunoblot experiments, three mice are shown per group.

Supplementary Materials

This PDF file includes:

Figs. S1 to S9

Table S1

REFERENCES AND NOTES

- Crosby, B., Davis, S., Joshi, M., Jardine, J., Paul, M., Neola, N. D., Barnard, Ketogenic diets and chronic disease: Weighing the benefits against the risks. *Front. Nutr.* **8**, 702802 (2021).
- Chun, K.-C., Ma, S.-C., Oh, H., Oh, J. M., Rho, D. Y., Kim, Ketogenic diet-induced extension of longevity in epileptic *Kcn1*-null mice is influenced by gender and age at treatment onset. *Epilepsia Res.* **140**, 53–55 (2018).
- Ko, G. J., Rhee, C. M., Kalandar-Zadeh, S., Joshi, The effects of high-protein diets on kidney health and longevity. *J. Am. Soc. Nephrol.* **31**, 1667–1679 (2020).
- Neal, E. G., Chaffe, R. H., Schwartz, M. S., Lawson, N., Edwards, G., Fitzsimmons, A., Whitney, J. H., Cross, The ketogenic diet for the treatment of childhood epilepsy: A randomised controlled trial. *Lancet Neurol.* **7**, 500–506 (2008).
- Allen, B. G., Bhatia, S. K., Bhatia, C. M., Anderson, J. M., Eichenberger-Gilmore, Z. A., Sibenaller, K. A., Mapuskar, J. D., Schoenfeld, J. M., Buatti, D. R., Spitz, M. A., Fath, Ketogenic diets as an adjuvant cancer therapy: History and potential mechanism. *Redox Biol.* **2**, 963–970 (2014).
- Stafstrom, C. E., Rho, J. M., The ketogenic diet as a treatment paradigm for diverse neurological disorders. *Front. Pharmacol.* **3**, 59 (2012).
- Gough, S. M., Casella, K. J., Ortega, A. S., Hackam, Neuroprotection by the ketogenic diet: Evidence and controversies. *Front. Nutr.* **8**, 782657 (2021).
- Ang, Q. Y., Alexander, J. C., Newman, Y. Tian, J. Cai, V. Upadhyay, J. A. Turnbaugh, E. Verdin, K. D. Hall, R. L. Leibel, E. Ravussin, M. Rosenbaum, A. D. Patterson, P. J. Turnbaugh, Ketogenic diets alter the gut microbiome resulting in decreased intestinal Th17 cells. *Cell* **181**, 1263–1275.e16 (2020).
- Goldberg, E. L., Shchukina, I. L., Asher, S., Sidorov, M. N., Artyomov, V. D., Dixit, Ketogenesis activates metabolically protective $\gamma\delta$ T cells in visceral adipose tissue. *Nat. Metab.* **2**, 50–61 (2020).
- Newman, J. C., Covarrubias, M., Zhao, X., Yu, P., Gut, C. P., Ng, Y., Huang, S., Haldar, E., Verdin, Ketogenic diet reduces midlife mortality and improves memory in aging mice. *Cell Metab.* **26**, 547–557.e8 (2017).
- Roberts, M. N., Wallace, A. A., Tomilov, Z., Zhou, G. R., Marcotte, D., Tran, G., Perez, E., Gutierrez-Casado, S., Koike, T. A., Knotts, D. M., Imai, S. M., Griffey, K., Kim, K., Hagopian, M. Z., McMackin, F. G., Haj, K., Baar, G. A., Cortopassi, J. J., Lopez-Dominguez, A., ketogenic diet extends longevity and healthspan in adult mice. *Cell Metab.* **26**, 539–546.e5 (2017).
- Xu, Y., Jiang, C., Wu, J., Liu, P., Deng, Y., Zhang, B., Peng, Y., Zhu, Ketogenic diet ameliorates cognitive impairment and neuroinflammation in a mouse model of Alzheimer's disease. *CNS Neurosci. Ther.* **28**, 580–592 (2022).
- Zhang, W., Chen, S., Huang, X., Tong, H., Niu, L., Lu, Neuroprotective effect of a medium-chain triglyceride ketogenic diet on MPTP-induced Parkinson's disease mice: A combination of transcriptomics and metabolomics in the substantia nigra and fecal microbiome. *Cell Death Discov.* **9**, 251 (2023).
- Youm, Y. H., Nguyen, K. Y., Nguyen, R. W., Grant, E. L., Goldberg, M., Bodogai, D., Kim, D., D'Agostino, N., Planavsky, C., Lupfer, T. D., Kanneganti, S., Kang, T. L., Horvath, T. M., Fahmy, P. A., Crawford, A., Biragyn, E., Alnemri, V. D., Dixit, The ketone metabolite β -hydroxybutyrate blocks NLRP3 inflammasome-mediated inflammatory disease. *Nat. Med.* **21**, 263–269 (2015).
- Asrih, M., Altirriba, F., Rohner-Jeanrenaud, F. R., Jornayvaz, Ketogenic diet impairs FGF21 signaling and promotes differential inflammatory responses in the liver and white adipose tissue. *PLOS ONE* **10**, e0126364 (2015).
- Li, S., Zhuge, A., Wang, L., Lv, X., Bian, L., Yang, J., Xia, X., Jiang, W., Wu, S., Wang, Q., Wang, L., Li, Ketogenic diet aggravates colitis, impairs intestinal barrier and alters gut microbiota and metabolism in DSS-induced mice. *Food Funct.* **12**, 10210–10225 (2021).
- Sternberg, C., Sternberg, A., Dunkel, T., Beikbaghban, A., Gregor, A., Szarzynski, V., Somoza, I., Walter, K., Duszka, B., Kofler, E. E., Pohl, Ketogenic diets composed of long-chain and medium-chain fatty acids induce cardiac fibrosis in mice. *Mol. Metab.* **72**, 101711 (2023).
- Xu, S., Tao, H., Cao, W., Cao, L., Cao, Y., Lin, S. M., Zhao, W., Xu, J., Cao, J. Y., Zhao, Ketogenic diets inhibit mitochondrial biogenesis and induce cardiac fibrosis. *Signal Transduct. Target. Ther.* **6**, 54 (2021).
- Jia, P., Huang, Y., You, H., Su, L., Gao, Ketogenic diet aggravates kidney dysfunction by exacerbating metabolic disorders and inhibiting autophagy in spontaneously hypertensive rats. *Biochem. Biophys. Res. Commun.* **573**, 13–18 (2021).
- Wallace, M. A., Aguirre, N. W., Marcotte, G. R., Marshall, A. G., Baehr, L. M., Baehr, D. C., Hughes, K. L., Hamilton, M. N., Roberts, J. A., Lopez-Dominguez, B. F., Miller, J. J., Ramsey, K., Baar, The ketogenic diet preserves skeletal muscle with aging in mice. *Aging Cell* **20**, e13322 (2021).
- Miles, K. N., Skelton, M. R., Male mice placed on a ketogenic diet from postnatal day (P) 21 through adulthood have reduced growth, are hypoactive, show increased freezing in a conditioned fear paradigm, and have spatial learning deficits. *Brain Res.* **1734**, 146697 (2020).
- Long, M. R., Bhatti, A., Kellenberger, W., Sun, S., Modica, M., Horing, G., Liebisch, J. P., Krieger, C., Wolfrum, T. D., Challa, A low-carbohydrate diet induces hepatic insulin resistance and metabolic associated fatty liver disease in mice. *Mol. Metab.* **69**, 101675 (2023).
- Batch, J. T., Lamsal, S. P., Adkins, M., Sultan, M. N., Ramirez, Advantages and disadvantages of the ketogenic diet: A review article. *Cureus* **12**, e9639 (2020).
- Kossoff, E. H., Zupec-Kania, B. A., Rho, M. J., Ketogenic diets: An update for child neurologists. *J. Child Neurol.* **24**, 979–988 (2009).
- Murphy, P., Use of the ketogenic diet as a long-term treatment for intractable epilepsy. *Dev. Med. Child Neurol.* **48**, 949 (2006).
- Groesbeck, D. K., Bluml, R. M., Kossoff, E. H., Long-term use of the ketogenic diet in the treatment of epilepsy. *Dev. Med. Child Neurol.* **48**, 978–981 (2006).
- Sturmlechner, M., Durik, C. J., Sieben, D. J., Baker, J. M., van Deursen, Cellular senescence in renal ageing and disease. *Nat. Rev. Nephrol.* **13**, 77–89 (2017).
- Mylonas, K. J., O'Sullivan, E. D., Humphries, D. P., Baird, M. H., Docherty, S. A., Neely, P. J., Krimpenfort, A., Melk, R., Schmitt, S., Ferreira-Gonzalez, S. J., Forbes, J., Hughes, D. A., Ferenbach, Cellular senescence inhibits renal regeneration after injury in mice, with senolytic treatment promoting repair. *Sci. Transl. Med.* **13**, eabb0203 (2021).

29. M. Mehdizadeh, M. Aguilar, E. Thorin, G. Ferbeyre, S. Nattel, The role of cellular senescence in cardiac disease: Basic biology and clinical relevance. *Nat. Rev. Cardiol.* **19**, 250–264 (2022).
30. M. Kozlowski, A. G. Ladurner, ATM, MacroH2A.1, and SASP: The checks and balances of cellular senescence. *Mol. Cell* **59**, 713–715 (2015).
31. M. Sadaie, R. Salama, T. Carroll, K. Tomimatsu, T. Chandra, A. R. Young, M. Narita, P. A. Perez-Mancera, D. C. Bennett, H. Chong, H. Kimura, M. Narita, Redistribution of the Lamin B1 genomic binding profile affects rearrangement of heterochromatic domains and SAHF formation during senescence. *Genes Dev.* **27**, 1800–1808 (2013).
32. S. Cui, L. Xue, F. Yang, S. Dai, Z. Han, K. Liu, B. Liu, Q. Yuan, Z. Cui, Y. Zhang, F. Xu, Y. Chen, Postinfarction hearts are protected by premature senescent cardiomyocytes via GATA 4-dependent CCN 1 secretion. *J. Am. Heart Assoc.* **7**, e009111 (2018).
33. Y. Cai, H. Zhou, Y. Zhu, Q. Sun, Y. Ji, A. Xue, Y. Wang, W. Chen, X. Yu, L. Wang, H. Chen, C. Li, T. Luo, H. Deng, Elimination of senescent cells by β -galactosidase-targeted prodrug attenuates inflammation and restores physical function in aged mice. *Cell Res.* **30**, 574–589 (2020).
34. M. A. Seol, U. Jung, H. S. Eom, S. H. Kim, H. R. Park, S. K. Jo, Prolonged expression of senescence markers in mice exposed to gamma-irradiation. *J. Vet. Sci.* **13**, 331–338 (2012).
35. J. H. Ellenbroek, L. van Dijck, H. A. Töns, T. J. Rabelink, F. Carlotti, B. E. P. B. Ballieux, E. J. P. de Koning, Long-term ketogenic diet causes glucose intolerance and reduced β - and α -cell mass but no weight loss in mice. *Am. J. Physiol. Endocrinol. Metab.* **306**, E552–E558 (2014).
36. A. L. Seufert, J. W. Hickman, J. Choi, B. A. Napier, Computational analysis of plasma lipidomics from mice fed standard chow and ketogenic diet. *Bio Protoc.* **13**, e4819 (2023).
37. M. Mijit, V. Caracciolo, A. Melillo, F. Amicarelli, A. Giordano, Role of p53 in the regulation of cellular senescence. *Biomolecules* **10**, 420 (2020).
38. R. Bernardi, P. P. Scaglioni, S. Bergmann, H. F. Horn, K. H. Vousden, P. P. Pandolfi, PML regulates p53 stability by sequestering Mdm2 to the nucleolus. *Nat. Cell Biol.* **6**, 665–672 (2004).
39. J. Loughery, M. Cox, L. M. Smith, D. W. Meek, Critical role for p53-serine 15 phosphorylation in stimulating transactivation at p53-responsive promoters. *Nucleic Acids Res.* **42**, 7666–7680 (2014).
40. R. G. Jones, D. R. Plas, S. Kubek, M. Buzzai, J. Mu, Y. Xu, M. J. Birnbaum, C. B. Thompson, AMP-activated protein kinase induces a p53-dependent metabolic checkpoint. *Mol. Cell* **18**, 283–293 (2005).
41. X. Tang, M. Miliavsky, N. Goldfinger, V. Rotter, Amyloid- β precursor-like protein APLP1 is a novel p53 transcriptional target gene that augments neuroblastoma cell death upon genotoxic stress. *Oncogene* **26**, 7302–7312 (2007).
42. E. Gonzalez-Gualda, A. G. Baker, L. Fruk, D. Munoz-Espin, A guide to assessing cellular senescence in vitro and in vivo. *FEBS J.* **288**, 56–80 (2021).
43. A. Freund, R. M. Laberge, M. Demaria, J. Campisi, Lamin B1 loss is a senescence-associated biomarker. *Mol. Biol. Cell* **23**, 2066–2075 (2012).
44. T. Jacks, L. Remington, B. O. Williams, E. M. Schmitt, S. Halachmi, R. T. Bronson, R. A. Weinberg, Tumor spectrum analysis in p53-mutant mice. *Curr. Biol.* **4**, 1–7 (1994).
45. H. I. Wettersten, S. Hee Hwang, C. Li, E. Y. Shiu, A. T. Wecksler, B. D. Hammock, R. H. Weiss, A novel p21 attenuator which is structurally related to sorafenib. *Cancer Biol. Ther.* **14**, 278–285 (2013).
46. J. Momand, G. P. Zambetti, D. C. Olson, D. George, A. J. Levine, The mdm-2 oncogene product forms a complex with the p53 protein and inhibits p53-mediated transactivation. *Cell* **69**, 1237–1245 (1992).
47. S. N. Jones, A. E. Roe, L. A. Donehower, A. Bradley, Rescue of embryonic lethality in Mdm2-deficient mice by absence of p53. *Nature* **378**, 206–208 (1995).
48. S. Janssens, A. Tinel, The PIDDosome, DNA-damage-induced apoptosis and beyond. *Cell Death Differ.* **19**, 13–20 (2012).
49. A. Tinel, J. Tschopp, The PIDDosome, a protein complex implicated in activation of caspase-2 in response to genotoxic stress. *Science* **304**, 843–846 (2004).
50. R. V. Talanian, C. Quinlan, S. Trautz, M. C. Hackett, J. A. Mankovich, D. Banach, T. Ghayur, K. D. Brady, W. W. Wong, Substrate specificities of caspase family proteases. *J. Biol. Chem.* **272**, 9677–9682 (1997).
51. F. Chen, Y. He, Caspase-2 mediated apoptotic and necrotic murine macrophage cell death induced by rough Brucella abortus. *PLOS ONE* **4**, e6830 (2009).
52. M. Poreba, K. Groborz, M. Navarro, S. J. Snipes, M. Drag, G. S. Salvesen, Caspase selective reagents for diagnosing apoptotic mechanisms. *Cell Death Differ.* **26**, 229–244 (2019).
53. L. Bergeron, G. I. Perez, G. Macdonald, L. Shi, Y. Sun, A. Jurisicova, S. Varmuza, K. E. Latham, J. A. Flaws, J. C. Salter, H. Hara, M. A. Moskowitz, E. Li, A. Greenberg, J. L. Tilly, J. Yuan, Defects in regulation of apoptosis in caspase-2-deficient mice. *Genes Dev.* **12**, 1304–1314 (1998).
54. V. J. Miller, F. A. Villamena, J. S. Volek, Nutritional ketosis and mitohormesis: Potential implications for mitochondrial function and human health. *J. Nutr. Metab.* **2018**, 5157645 (2018).
55. D. M. Thomson, W. W. Winder, AMP-activated protein kinase control of fat metabolism in skeletal muscle. *Acta Physiol.* **196**, 147–154 (2009).
56. K. Beyfuss, D. A. Hood, A systematic review of p53 regulation of oxidative stress in skeletal muscle. *Redox Rep.* **23**, 100–117 (2018).
57. X. Liu, R. R. Chhipa, I. Nakano, B. Dasgupta, The AMPK inhibitor compound C is a potent AMPK-independent antiangioma agent. *Mol. Cancer Ther.* **13**, 596–605 (2014).
58. T. G. Oliver, E. Meylan, G. P. Chang, W. Xue, J. R. Burke, T. J. Humpton, D. Hubbard, A. Bhutkar, T. Jacks, Caspase-2-mediated cleavage of Mdm2 creates a p53-induced positive feedback loop. *Mol. Cell* **43**, 57–71 (2011).
59. B. G. Childs, M. Gluscevic, D. J. Baker, R. M. Laberge, D. Marques, J. Dananberg, J. M. van Deursen, Senescent cells: An emerging target for diseases of aging. *Nat. Rev. Drug Discov.* **16**, 718–735 (2017).
60. R. Di Micco, V. Krizhanovsky, D. Baker, F. d'Adda di Fagagna, Cellular senescence in aging: From mechanisms to therapeutic opportunities. *Nat. Rev. Mol. Cell Biol.* **22**, 75–95 (2021).
61. X. Li, C. Li, W. Zhang, Y. Wang, P. Qian, H. Huang, Inflammation and aging: Signaling pathways and intervention therapies. *Signal Transduct. Target. Ther.* **8**, 239 (2023).
62. Y. Du, J. Wang, S. Li, B. Dennis, C. Meireles, N. Siddiqui, D. Patel, J. Gelfond, C. Li, S. H. Faruqui, A. Alaezdi, V. Drel, J. Tumova, H. Ye, R. Montellano, G. Armaiz-Pena, K. Sharma, A technology assisted precision ketogenic diet intervention for cardio-renal-metabolic health in overweight or obese adults: Protocol for a randomized controlled trial. *Contemp. Clin. Trials* **119**, 106845 (2022).
63. J. Chang, Y. Wang, L. Shao, R. M. Laberge, M. Demaria, J. Campisi, K. Janakiraman, N. E. Sharpless, S. Ding, W. Feng, Y. Luo, X. Wang, N. Aykin-Burns, K. Krager, U. Ponnappan, M. Hauer-Jensen, A. Meng, D. Zhou, Clearance of senescent cells by ABT263 rejuvenates aged hematopoietic stem cells in mice. *Nat. Med.* **22**, 78–83 (2016).
64. Y. Guo, X. Liu, T. Li, J. Zhao, Y. Yang, Y. Yao, L. Wang, B. Yang, G. Ren, Y. Tan, S. Jiang, Alternate-day ketogenic diet feeding protects against heart failure through preservation of ketogenesis in the liver. *Oxid. Med. Cell. Longev.* **2022**, 4253651 (2022).
65. C. F. Kirkpatrick, J. P. Bolick, P. M. Kris-Etherton, G. Sikand, K. E. Aspray, D. E. Soffer, K. E. Willard, K. C. Maki, Review of current evidence and clinical recommendations on the effects of low-carbohydrate and very-low-carbohydrate (including ketogenic) diets for the management of body weight and other cardiometabolic risk factors: A scientific statement from the National Lipid Association Nutrition and Lifestyle Task Force. *J. Clin. Lipidol.* **13**, 689–711.e1 (2019).
66. T. Shimazu, M. D. Hirschey, J. Newman, W. He, K. Shirakawa, N. Le Moan, C. A. Grueter, H. Lim, L. R. Saunders, R. D. Stevens, C. B. Newgard, R. V. Farese Jr., R. de Cabo, S. Ulrich, K. Akassoglou, E. Verdin, Suppression of oxidative stress by β -Hydroxybutyrate, an endogenous histone deacetylase inhibitor. *Science* **339**, 211–214 (2013).
67. J. Tao, H. Chen, Y. J. Wang, J. X. Qiu, Q. Q. Meng, R. J. Zou, L. Li, J. G. Huang, Z. K. Zhao, Y. L. Huang, H. F. Zhang, J. M. Zheng, Ketogenic diet suppressed T-regulatory cells and promoted cardiac fibrosis via reducing mitochondria-associated membranes and inhibiting mitochondrial function. *Oxid. Med. Cell. Longev.* **2021**, 5512322 (2021).
68. H. Tuunanen, J. Knuuti, Metabolic remodelling in human heart failure. *Cardiovasc. Res.* **90**, 251–257 (2011).
69. I. Shimizu, T. Minamino, Cellular senescence in cardiac diseases. *J. Cardiol.* **74**, 313–319 (2019).
70. J. Mercer, M. Bennett, The role of p53 in atherosclerosis. *Cell Cycle* **5**, 1907–1909 (2006).
71. A. Corcello, C. M. Trovato, E. Di Profio, S. Cardile, C. Campoy, G. Zuccotti, E. Verduci, A. Diamanti, Ketogenic diet in children and adolescents: The effects on growth and nutritional status. *Pharmacol. Res.* **191**, 106780 (2023).
72. K. Newmaster, Z. Zhu, E. Bolt, R. J. Chang, C. Day, A. Mhanna, S. Paudel, O. Farooq, A. Swaminathan, P. Acharya, W. Cheungpasitporn, S. Gupta, D. Samanta, N. Mahfooz, G. Mainali, P. R. Carney, S. Naik, A review of the multi-systemic complications of a ketogenic diet in children and infants with epilepsy. *Children* **9**, 1372 (2022).
73. H. C. Kang, D. E. Chung, D. W. Kim, H. D. Kim, Early- and late-onset complications of the ketogenic diet for intractable epilepsy. *Epilepsia* **45**, 1116–1123 (2004).
74. Z. Zhou, K. Kim, J. J. Ramsey, J. M. Rutkowsky, Ketogenic diets initiated in late mid-life improved measures of spatial memory in male mice. *Geroscience* **45**, 2481–2494 (2023).
75. H. S. Kim, K. Patel, K. Muldoon-Jacobs, K. S. Bisht, N. Aykin-Burns, J. D. Pennington, R. van der Meer, P. Nguyen, J. Savage, K. M. Owens, A. Vassilopoulos, O. Ozden, S. H. Park, K. K. Singh, S. A. Abdulkadir, D. R. Spitz, C. X. Deng, D. Gius, SIRT3 is a mitochondria-localized tumor suppressor required for maintenance of mitochondrial integrity and metabolism during stress. *Cancer Cell* **17**, 41–52 (2010).
76. R. Tao, M. C. Coleman, J. D. Pennington, O. Ozden, S. H. Park, H. Jiang, H. S. Kim, C. R. Flynn, S. Hill, W. Hayes McDonald, A. K. Olivier, D. R. Spitz, D. Gius, Sirt3-mediated deacetylation of evolutionarily conserved lysine 122 regulates MnSOD activity in response to stress. *Mol. Cell* **40**, 893–904 (2010).
77. L. V. Popova, P. Nagarajan, C. M. Lovejoy, B. D. Sunkel, M. L. Gardner, M. Wang, M. A. Freitas, B. Z. Stanton, M. R. Parthun, Epigenetic regulation of nuclear lamina-associated heterochromatin by HAT1 and the acetylation of newly synthesized histones. *Nucleic Acids Res.* **49**, 12136–12151 (2021).

Acknowledgments**Funding:** This work was supported by the National Cancer Institute, grants R01CA152601

(D.G.), R01CA214025 (D.G.), and U01CA268813 (J.C.); National Cancer Institute R01 supplements, R01CA214025-05 (E.S.C.) and R01CA257148 (R.T.); National Institute on Aging, training grant T32AG021890-20 (J.R.S.); Cancer Prevention and Research Institute of Texas, grants RR20012 (D.G.) and RP220650 (J.C.); Breast Cancer Research Foundation (J.C.); Philanthropic support from M. Neal and R. Neal (J.C.); 80/20 Foundation (K.S.); and Barshop Institute of Longevity and Aging Nathan Shock Centers of Excellence. **Author contributions:** Conceptualization: S.-J.W., N.H., and D.G. Methodology: S.-J.W., M.V., G.X., W.H.C., G.M.M., P.S., Y.D., J.C., N.H., and D.G. Software: J.R.S. Validation: S.-J.W., M.V., W.H.C., R.T., K.S., N.H., and D.G. Formal analysis: S.-J.W., J.R.S., A.N., W.Q., B.L., E.M., and D.G. Investigation: S.-J.W., J.R.S., E.S.C., M.V., G.X., W.H.C., P.S., R.T., W.Q., G.M.M., F.F.D., B.L., A.N., Y.D., A.S., and K.S. Resources: S.-J.W., M.V., F.F.D., W.Q., Y.D., A.S., K.S., J.C., N.H., and D.G. Data curation: S.-J.W. and J.R.S. Writing—original draft: S.-J.W., J.R.S., M.V., E.M., N.H., and D.G.

Writing—review and editing: S.-J.W., J.R.S., E.S.C., E.M., J.C., K.S., N.H., and D.G. Visualization: S.-J.W., J.R.S., E.S.C., E.M., N.H., and D.G. Supervision: S.-J.W., M.V., H.J., J.C., W.Q., K.S., N.H., and D.G. Project administration: S.-J.W., H.J., W.H.C., R.T., W.Q., K.S., N.H., and D.G. Funding acquisition: J.C., K.S., and D.G. **Competing interests:** The authors declare that they have no competing interests. **Data and materials availability:** All data needed to evaluate the conclusions in the paper are present in the paper and/or the Supplementary Materials. The accession number for the RNA-seq data is GEO: GSE233831.

Submitted 19 January 2024

Accepted 12 April 2024

Published 17 May 2024

10.1126/sciadv.ado1463